

RESEARCH ARTICLE

WILEY

A refinement approach to the multivariable tracking error problem

Arnold Pretorius¹ | Edward Boje²

Department of Electrical Engineering,
University of Cape Town, Cape Town,
Western Cape, South Africa

Correspondence

Arnold Pretorius, Department of
Electrical Engineering, University of Cape
Town, Cape Town, Western Cape 7700,
South Africa

Email: prtarn001@myuct.ac.za

Funding information

South African National Research
Foundation, Grant/Award Number: 81148

Abstract

This article presents a new refinement design routine aimed at solving the robust multivariable tracking error problem with reduced conservatism. The prevailing multivariable quantitative feedback theory (QFT) approach is to implicitly over-bound the model-error tracking set frequency response in magnitude using the triangle inequality, with the intention of arriving at a set of univariate design constraints that independently describe the feedback controller solution space. While this method is effective in the low-frequency range (where the loop gain tends to be large), the mid- to high-frequency design regions (where diagonal dominance is not possible in general) suffers from arbitrarily large design conservatism. This inhibits minimum gain-phase solutions and necessitates undesirable over-design in the frequency band that can contribute to large, expensive control action. The proposed method follows a refinement approach that makes use of information from an a priori feedback control design. In this way, the tracking error problem is reposed as a differential design, and gain-phase information from the previous iteration can be captured to reduce the conservatism imposed when applying the triangle inequality. Additionally, a constrained optimization routine is used to select a prototype feedforward filter that can relax the constraint set, thereby increasing the accessible solution space of the diagonal feedback controller. Finally, a nondiagonal, multivariable feedforward filter bound generation routine is defined that relies on existence conditions and is free of induced design conservatism. The viability of this design methodology is demonstrated on two benchmark problems of varying complexity, in order to demonstrate the widespread efficacy.

KEYWORDS

MIMO QFT, robust control, tracking error specifications

1 | INTRODUCTION

Within the QFT research sphere, the multivariable tracking problem has been met with varying efficacy.¹ Broadly speaking, the two approaches are to either (i) apply above/below tracking magnitude bounds,² or (ii) use tracking error bounds.³ Research that falls under (i) has benefit in being computationally simpler, but commonly requires a diagonal prefilter

Abbreviations: QFT, quantitative feedback theory; SISO, single-input-single-output; MIMO, multi-input-multi-output; 2DOF, two-degree-of-freedom.

This is an open access article under the terms of the Creative Commons Attribution-NonCommercial-NoDerivs License, which permits use and distribution in any medium, provided the original work is properly cited, the use is non-commercial and no modifications or adaptations are made.

© 2022 The Authors. *International Journal of Robust and Nonlinear Control* published by John Wiley & Sons Ltd.

to facilitate the design. Work in Reference 4 uses the classical approach of under- and over-bounding the closed-loop behavior to design a diagonal prefilter and feedback controller for a 2×2 heat exchanger. Additionally, the way in which tracking tolerances couple across the design loops is exploited to tighten constraints on a particular loop whilst relaxing the constraints in the other loops. This has the benefit that, when chosen appropriately, nondominant boundaries in one channel will become stricter, but remain nondominant, whilst easing the dominant boundaries in the other channels. As noted in Reference 5, there is benefit in having a fully populated prefilter, as it can aid in the loop decoupling and reduce the burden on the feedback controller elements. Additionally, there is the potential for diminished time-domain tracking precision as a result of not capturing relative phase information between the closed-loop system and above/below specifications.⁶ The more recent introduction of multivariable tracking error bounding methods has comparable magnitude boundaries on the closed-loop system, but additionally imposes differential phase constraints.⁷ A common approach is to predefine the prefilter using information from an appropriately selected nominal plant.³ This removes one degree of freedom from the control scheme and allows for direct design on the feedback controller elements when using plant-inverting splittings. The work in Reference 8 additionally proposes a refinement of the prefilter once the feedback controller has been designed, which can alleviate the burden of implementing a potentially irrational or ill-conditioned prefilter. While this design procedure is computationally simple, the suboptimal prefilter synthesis can place additional design conservatism on the feedback controller. This is worsened by the fact that the nominal plant selection is not obvious for complex systems with irregular uncertainty template shapes, and this can exacerbate the contracted feedback controller solution space.⁹ A less conservative routine was proposed in Reference 10, which separates the tracking error problem into a simultaneous tracking and disturbance rejection problem using iterative bound balancing methods. This design method allows for a fully populated prefilter, and the design regions are independent of the nominal plant selection. This method is similarly implemented for the measured disturbance rejection problem in Reference 11. The aforementioned design routines all rely on using a plant-inverting splitting, which can incur large design conservatism at the mid-to high-frequencies as a result of poor loop diagonal dominance.¹² More recently, a complementary design routine was proposed that combines a plant-inverting design with a nonplant-inverting design.⁹ This method is able to reduce design conservatism at all frequencies, especially at and above the gain-crossover frequency, but only applies to the special case of 2×2 systems.

The state of the art of multivariable QFT is fundamentally limited by having to assume a worst-case gain-phase over-bounding of the tracking error matrix when applying the triangle inequality. If knowledge of a prior valid design were known, the corresponding phase and gain information could be captured, thereby reducing the amount of over-bounding required. This paper seeks to exploit the design insight from this relationship to repose the tracking error constraint set in a form that incrementally increases the feedback controller design regions. Information from a successful feedback controller refinement is then incorporated into a subsequent feedback control design pass, which reduces the amount of conservatism on the feedback controller elements incurred when using the triangle inequality. Following the successful design of the feedback controller, the solution space of one row of the feedforward filter is ipso facto defined, based on the existential link between the feedback controller and feedforward filter. Existence conditions are then chained to sequentially design each row of the feedforward filter. While informed from the feedback controller selection, the solution space of the feedforward filter is evaluated without using overbounding and does not carry any induced conservatism. As this method is a QFT design tool that finds feasible regions at discrete design frequency points, the designer is still required to join these regions with a sufficiently low-order, causal controller, capable of achieving closed-loop plant stability. This is a generalized design method that is applicable to $n \times n$ systems, and is bench-marked using two different 2×2 plants of varying complexity, for sake of clarity and demonstration.

2 | PROBLEM STATEMENT

Consider the two degree of freedom (2DOF) control configuration of Figure 1, where $P^i(s) \in \mathcal{P}(s)$ is an $m \times m$ plant instance in the uncertain set $\mathcal{P}(s)$; $r(s)$ is the $m \times 1$ reference signal; and $M(s)$ is the $m \times m$ reference model that describes the ideal closed-loop transfer behavior. Set $\mathcal{P}(s) = \{P^1(s), P^2(s), \dots, P^n(s)\}$ is an ϵ -net of disjoint plants that sufficiently describes the uncertain plant. Diagonal feedback controller $G(s) = \text{diag}\{g_1(s), g_2(s), \dots, g_m(s)\}$ acts to reduce uncertainty across the plant set, while $m \times m$ feedforward filter $X(s)$ is designed to adjust the closed-loop bandwidth of the plant set and distribute reference signal information across the control loops.

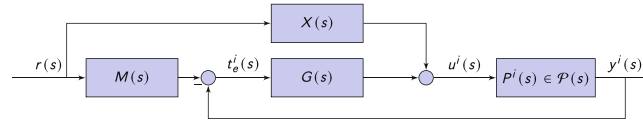


FIGURE 1 Block diagram of feedback-feedforward control scheme for plant instance i , with two degrees of freedom, $\{G(s), X(s)\}$

The structure in Figure 1 is analogous to traditional prefilter approaches, as seen in Reference 1 for example, with the notable benefit that it inherently captures the reference model tracking error within the loop:

$$t_e^i(s) = M(s)r(s) - y^i(s) = E^i(s)r(s), \quad (1)$$

where

$$E^i(s) = [I + P^i(s)G(s)]^{-1} (M(s) - P^i(s)X(s)). \quad (2)$$

Following standard quantitative feedback tracking error methods,³ the element-wise magnitude of the matrix reference model tracking error frequency response in (2) can be constrained by a defined specification,

$$|e_{ab}^i(j\omega_d)| \leq \beta_{ab}(\omega_d), \quad (3)$$

where $\beta_{ab}(\omega_d)$ is the user-specified reference model tracking error tolerance at row a and column b , and $\omega_d \in \Omega$ is the discrete design frequency point of interest. The design frequency set, Ω , is chosen based on engineering understanding of the control problem, and is required to be sufficiently rich in order to capture the contiguous frequency behavior of the closed-loop system.¹³ The objective is to design $G(s)$ and $X(s)$ in (2) in order to meet the constraints of (3) for all plant cases, $i \in \{1, 2, \dots, n\}$. Additionally, cost-effective design requires that bandwidth minimization and simplicity of $G(s)$ be prioritized over that of $X(s)$.⁵

3 | METHOD

3.1 | Preliminary feedback control design

A preliminary $G(j\omega)$ prototype is required in order to proceed with the refinement process in Section 3.2. This $G(j\omega)$ can be obtained by any means, such as synthesis, with the only requirement being that a nonempty design region of the corresponding $X(j\omega)$ exists that can satisfy (3).

A preliminary feedback control design is proposed here as one applicable method and follows the existential plant-inverting method first introduced in Reference 9. Using the frequency response definition of $s = j\omega$, the tracking error for plant instance i follows from (2) as

$$E^i(j\omega) = [I + P^i(j\omega)G(j\omega)]^{-1} [M(j\omega) - P^i(j\omega)X(j\omega)]. \quad (4)$$

Assuming the plant inverse, $P^i(j\omega)^{-1} = \hat{P}^i(j\omega)$, is nonsingular at the chosen design frequencies, the conventional plant-inverting splitting approach¹⁴ is applied

$$[\hat{P}^i(j\omega) + G(j\omega)] E^i(j\omega) = \hat{P}^i(j\omega)M(j\omega) - X(j\omega). \quad (5)$$

The plant inverse is then separated into diagonal and off-diagonal parts respectively, $\hat{P}^i(j\omega) = \hat{P}_d^i(j\omega) + \hat{P}_n^i(j\omega)$, and the resulting equation is rearranged to give the implicit form of

$$\hat{P}^i(j\omega)M(j\omega) - X(j\omega) - \hat{P}_n^i(j\omega)E^i(j\omega) = [\hat{P}_d^i(j\omega) + G(j\omega)] E^i(j\omega). \quad (6)$$

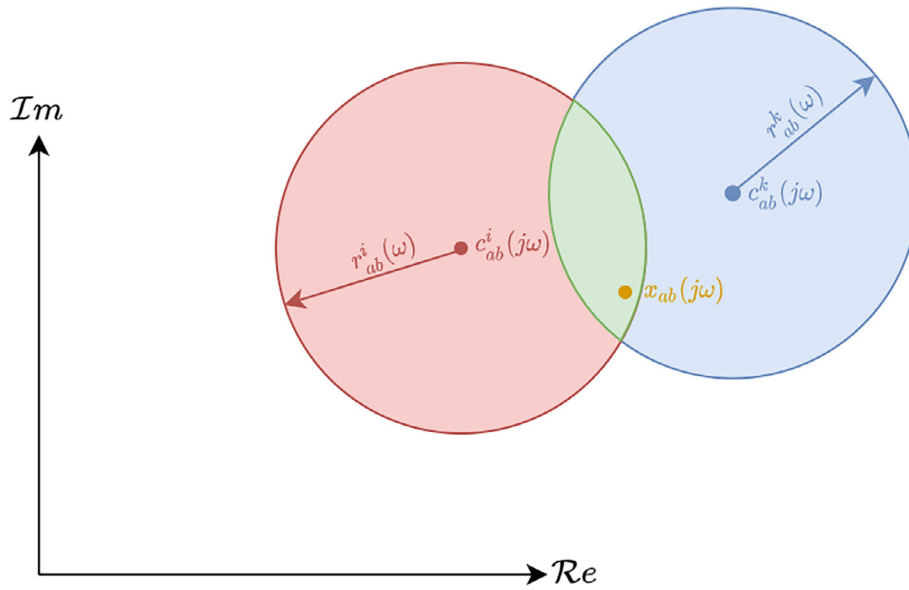


FIGURE 2 Visual representation of two discoidal *stay-in* design regions of $x_{ab}(j\omega)$ in the arithmetic-complex plane. Each plant instance generates a *stay-in* disc from (8), and a viable solution of $x_{ab}(j\omega)$ is required to lie within the intersection of the two discs. Existence of a nonempty intersection is predicated upon satisfying $\left|c_{ab}^i - c_{ab}^k\right|_{\omega} \leq r_{ab}^i(\omega) + r_{ab}^k(\omega)$.

Given the element-wise matrix magnitude constraint of $|E|_{\omega}^i \leq \beta(\omega)$ from (3), where

$$|E|_{\omega}^i = \begin{bmatrix} |e_{11}^i(j\omega)| & |e_{12}^i(j\omega)| & \dots & |e_{1m}^i(j\omega)| \\ |e_{21}^i(j\omega)| & |e_{22}^i(j\omega)| & & \vdots \\ \vdots & & \ddots & \\ |e_{m1}^i(j\omega)| & \dots & & |e_{mm}^i(j\omega)| \end{bmatrix}, \quad (7)$$

the nonconservative tracking constraint related to (6) is posed as

$$\left| \hat{P}^i M - \hat{P}_n^i E^i - X \right|_{\omega} \leq \left| \hat{P}_d^i + G \right|_{\omega} \beta(\omega). \quad (8)$$

Rewriting (8) compactly as $|C^i - X|_{\omega} \leq R^i(\omega)$, where $C^i(j\omega) = \left[\hat{P}^i M - \hat{P}_n^i E^i \right]_{\omega}$ and $R^i(\omega) = \left| \hat{P}_d^i + G \right|_{\omega} \beta(\omega)$, the i th plant solution space of $x_{ab}(j\omega)$ —the element of $X(j\omega)$ at row a and column b —is a *stay-in* disc, with a center of $c_{ab}^i(j\omega)$, and a radius of $r_{ab}^i(\omega)$, as shown in Figure 2. Generalized nonsingleton plant sets require that every plant-instanced *stay-in* disc of $x_{ab}(j\omega)$ has a common overlap, thereby guaranteeing that a nonempty set of $x_{ab}(j\omega)$ points exist in the arithmetic-complex plane that can simultaneously satisfy the constraint set in (8) for two different plant cases. With reference to Figure 2 and Reference 15, this necessitates that the distance between any two plant-instanced centers must be smaller than or equal to the sum of their corresponding radii $\left|c_{ab}^i - c_{ab}^k\right|_{\omega} \leq r_{ab}^i(\omega) + r_{ab}^k(\omega)$. The element-wise matrix equivalent, $|C^i - C^k|_{\omega} \leq R^i(\omega) + R^k(\omega)$, follows as

$$\left| (\hat{P}^i - \hat{P}^k) M + \hat{P}_n^k E^k - \hat{P}_n^i E^i \right|_{\omega} \leq \left[|\hat{P}_d^i + G|_{\omega} + |\hat{P}_d^k + G|_{\omega} \right] \beta(\omega), \quad \forall i, k \in [1, n]. \quad (9)$$

Note that (9) is a necessary but not sufficient condition for an $X(j\omega)$ to exist across the entire plant set, as there is no guarantee that a common intersection exists for all *stay-in* discs. The plant-instanced tracking error matrices— $E^i(j\omega)$ and $E^k(j\omega)$ in (9)—are unknown prior to fixing $G(j\omega)$ and $X(j\omega)$ and this necessitates over-bounding. Applying the triangle inequality to the left-hand side of (9), whilst grouping all known frequency response information, results in

$$\left| (\hat{P}^i - \hat{P}^k) M + \hat{P}_n^k E^k - \hat{P}_n^i E^i \right|_{\omega} \leq \left| (\hat{P}^i - \hat{P}^k) M \right|_{\omega} + \left(\left| \hat{P}_n^i \right|_{\omega} + \left| \hat{P}_n^k \right|_{\omega} \right) \beta(\omega). \quad (10)$$

Equation (10) is then used to form the conservative constraint of

$$\left| \left(\hat{P}^i - \hat{P}^k \right) M + \hat{P}_n^k E^k - \hat{P}_n^i E^i \right|_{\omega} \leq \left| \left(\hat{P}^i - \hat{P}^k \right) M \right|_{\omega} + \left(\left| \hat{P}_n^i \right|_{\omega} + \left| \hat{P}_n^k \right|_{\omega} \right) \beta(\omega) \leq \left(\left| \hat{P}_d^i + G \right|_{\omega} + \left| \hat{P}_d^k + G \right|_{\omega} \right) \beta(\omega), \quad (11)$$

where satisfying the right-hand inequality in (11) of

$$\left| \left(\hat{P}^i - \hat{P}^k \right) M \right|_{\omega} + \left(\left| \hat{P}_n^i \right|_{\omega} + \left| \hat{P}_n^k \right|_{\omega} \right) \beta(\omega) \leq \left(\left| \hat{P}_d^i + G \right|_{\omega} + \left| \hat{P}_d^k + G \right|_{\omega} \right) \beta(\omega), \quad \forall i, k \in [1, n] \quad (12)$$

will implicitly satisfy (9). The conservatism of the applied triangle inequality in (10) is problematic when $\left(\left| \hat{P}_n^i \right|_{\omega} + \left| \hat{P}_n^k \right|_{\omega} \right) \beta(\omega)$ is not small relative to $\left| \left(\hat{P}^i - \hat{P}^k \right) M \right|_{\omega}$ and results in diminished design regions for the diagonal elements of $G(j\omega)$, based on the structure in (12). This commonly occurs in the mid- to high-frequency band as a result of $\left| \hat{P}_n(j\omega) \right|$ rolling up while $M(j\omega)$ rolls off. Equation (12) is solely a function of decoupled $G(j\omega)$, and this allows for direct design of the feedback controller elements in a nonsequential manner. As detailed in Reference 9, the per-frequency plant-instanced design regions of $G(j\omega)$ in (12) are *stay-out* ellipses (when represented in the arithmetic-complex plane). Note that this bound generation constraint is comparable to the proposed approach in Reference 10, albeit with no requirement for iterative manual inspection and parameter adjustment. Additionally, because the method in Reference 10 does not attempt to balance the boundaries at every feedback controller phase angle, there will, in general, exist phase-dependent design regions where one design constraint dominates the other, thereby inducing additional conservatism relative to (12).

3.2 | Refining an existing design

In this article, we assume that there is a preliminary feedback controller design, $G_o(s)$, that gives rise to nonempty design regions for the frequency response of $X_o(s)$ at each design frequency. Adherence to the tracking specifications is verified by evaluating (4) at $X(j\omega) = X_o(j\omega)$ and $G(j\omega) = G_o(j\omega)$:

$$E_o^i(j\omega) = (I + P^i G_o)^{-1} (M - P^i X_o)|_{\omega}, \quad \forall i \in [1, n], \quad (13)$$

with the requirement that $|E_o^i|_{\omega} \leq \beta(\omega)$, $\forall i \in [1, n]$. The design conservatism in (12) is a result of having to take the worst-case gain and phase behavior of the implicit per-plant tracking error terms when applying the triangle inequality. If prior gain and phase information of the tracking error can be extracted from a preliminary controller design using (13), this can be incorporated into the constraint in (9) before applying the triangle inequality, with the objective of reducing the amount of overbounding. Defining $E^i(j\omega) = E_o^i(j\omega) + \Delta E^i(j\omega)$, (9) can be written as

$$\left| \left(\hat{P}^i - \hat{P}^k \right) M + \hat{P}_n^k (E_o^k + \Delta E^k) - \hat{P}_n^i (E_o^i + \Delta E^i) \right|_{\omega} \leq \left(\left| \hat{P}_d^i + G \right|_{\omega} + \left| \hat{P}_d^k + G \right|_{\omega} \right) \beta(\omega), \quad \forall i, k \in [1, n]. \quad (14)$$

While the corresponding incremental feedback design follows as $G(j\omega) = G_o(j\omega) + \Delta G(j\omega)$, boundaries are derived on absolute $G(j\omega)$ without loss of generality. Applying the triangle inequality to the left-hand side of (14), while retaining all known frequency response information in the first term, results in

$$\left| \left(\hat{P}^i - \hat{P}^k \right) M + \hat{P}_n^k (E_o^k + \Delta E^k) - \hat{P}_n^i (E_o^i + \Delta E^i) \right|_{\omega} \leq \left| \left(\hat{P}^i - \hat{P}^k \right) M + \hat{P}_n^k E_o^k - \hat{P}_n^i E_o^i \right|_{\omega} + \left| \hat{P}_n^i \right|_{\omega} \left| \Delta E^i \right|_{\omega} + \left| \hat{P}_n^k \right|_{\omega} \left| \Delta E^k \right|_{\omega}. \quad (15)$$

Equation 15 is then used to form the overbounded constraint set of

$$\left| \left(\hat{P}^i - \hat{P}^k \right) M + \hat{P}_n^k E_o^k - \hat{P}_n^i E_o^i \right|_{\omega} + \left| \hat{P}_n^i \right|_{\omega} \left| \Delta E^i \right|_{\omega} + \left| \hat{P}_n^k \right|_{\omega} \left| \Delta E^k \right|_{\omega} \leq \left(\left| \hat{P}_d^i + G \right|_{\omega} + \left| \hat{P}_d^k + G \right|_{\omega} \right) \beta(\omega), \quad \forall i, k \in [1, n], \quad (16)$$

where (16) is a sufficient condition in satisfying (14). $|\Delta E^i|_{\omega}$ is unknown and can be overbounded by $|\Delta E^i|_{\omega} \leq \Delta \beta(\omega)$, $\forall i \in [1, n]$, where $\Delta \beta(\omega) \geq 0$ is an adjustable parameter that is detailed in Section 3.2.1. The univariate design constraint set on $G(j\omega)$ follows as

$$\left| \left(\hat{P}^i - \hat{P}^k \right) M + \hat{P}_n^k E_o^k - \hat{P}_n^i E_o^i \right|_{\omega} + \left(\left| \hat{P}_n^i \right|_{\omega} + \left| \hat{P}_n^k \right|_{\omega} \right) \Delta \beta(\omega) \leq \left(\left| \hat{P}_d^i + G \right|_{\omega} + \left| \hat{P}_d^k + G \right|_{\omega} \right) \beta(\omega), \quad \forall i, k \in [1, n]. \quad (17)$$

While the right-hand side matrices in (12) and (17) are identical, the left-hand sides are different. Moreover, if $\Delta \beta(\omega) \leq \beta(\omega) - |E_o^i|_{\omega}$, $\forall i \in [1, n]$, then the left-hand side of (17) will be strictly smaller than or equal to the left-hand side of (12):

$$\left| \left(\hat{P}^i - \hat{P}^k \right) M + \hat{P}_n^k E_o^k - \hat{P}_n^i E_o^i \right|_{\omega} + \left(\left| \hat{P}_n^i \right|_{\omega} + \left| \hat{P}_n^k \right|_{\omega} \right) \Delta \beta(\omega) \leq \left| \left(\hat{P}^i - \hat{P}^k \right) M \right|_{\omega} + \left(\left| \hat{P}_n^i \right|_{\omega} + \left| \hat{P}_n^k \right|_{\omega} \right) \beta(\omega). \quad (18)$$

Denoting $A^{ik}(j\omega) = \left[\left(\hat{P}^i - \hat{P}^k \right) M + \hat{P}_n^k E_o^k - \hat{P}_n^i E_o^i \right]_{\omega}$ and noting that $\hat{P}_n^i(j\omega)$ is a hollow matrix, (17) can be represented in element-wise form as

$$\left| a_{rc}^{ik}(j\omega) \right| + \sum_{v=1, v \neq r}^m \left[\left| \hat{P}_{rv}^i \right| + \left| \hat{P}_{rv}^k \right| \right]_{\omega} \Delta \beta_{vc}(\omega) \leq \left(\left| \hat{P}_{rr}^i + g_r \right|_{\omega} + \left| \hat{P}_{rr}^k + g_r \right|_{\omega} \right) \beta_{rc}(\omega). \quad (19)$$

The overbounded element-wise tracking error constraint follows as

$$\frac{\left| a_{rc}^{ik}(j\omega) \right|}{\left| \hat{P}_{rr}^i + g_r \right|_{\omega} + \left| \hat{P}_{rr}^k + g_r \right|_{\omega}} + \frac{\sum_{v=1, v \neq r}^m \left[\left| \hat{P}_{rv}^i \right| + \left| \hat{P}_{rv}^k \right| \right]_{\omega} \Delta \beta_{vc}(\omega)}{\left| \hat{P}_{rr}^i + g_r \right|_{\omega} + \left| \hat{P}_{rr}^k + g_r \right|_{\omega}} \leq \beta_{rc}(\omega), \quad (20)$$

and is shown graphically in Figure 3. Dividing both sides of (19) by $\beta_{rc}(\omega)$ yields

$$\frac{\left| a_{rc}^{ik}(j\omega) \right|}{\beta_{rc}(\omega)} + \frac{\sum_{v=1, v \neq r}^m \left[\left| \hat{P}_{rv}^i \right| + \left| \hat{P}_{rv}^k \right| \right]_{\omega} \Delta \beta_{vc}(\omega)}{\beta_{rc}(\omega)} \leq \left| \hat{P}_{rr}^i + g_r \right|_{\omega} + \left| \hat{P}_{rr}^k + g_r \right|_{\omega}, \quad (21)$$

and geometrically describes an elliptical *stay-out* design region of $g_r(j\omega)$ for plant pair $\{i, k\}$, with foci at $-\hat{P}_{rr}^i(j\omega)$ and $-\hat{P}_{rr}^k(j\omega)$, and a corresponding major axis of $\gamma_{rc}(\omega) = \frac{\left| a_{rc}^{ik}(j\omega) \right|}{\beta_{rc}(\omega)} + \frac{\sum_{v=1, v \neq r}^m \left[\left| \hat{P}_{rv}^i \right| + \left| \hat{P}_{rv}^k \right| \right]_{\omega} \Delta \beta_{vc}(\omega)}{\beta_{rc}(\omega)}$, as seen in Figure 4. As such, reducing the left-hand side of (21) will monotonically expand the admissible design region of $G(j\omega)$. There are two mechanisms that can be used to achieve this, and these are detailed in Sections 3.2.1 and 3.2.2. With reference to Figure 4, feedback controller element $g_r(j\omega)$ will have m ellipses with coincident foci. As such, the union of the *stay-out* ellipses is equivalent to the ellipse with the largest major axis,

$$\max_{c \in [1, m]} \gamma_{rc} \leq \left| \hat{P}_{rr}^i + g_r \right|_{\omega} + \left| \hat{P}_{rr}^k + g_r \right|_{\omega}. \quad (22)$$

3.2.1 | Bounding the incremental error

As introduced in (17), $|\Delta E^i|_{\omega} \leq \Delta \beta(\omega)$ serves as an overbounding on the incremental error allowed, where the current error is $E_o^i(j\omega)$. It is tempting to reduce $\Delta \beta(\omega)$ in order to minimize the left-hand side in (17), but this places additional design strictures on $\Delta G(j\omega)$ that are not immediately apparent. In essence, constraining $\Delta \beta(\omega)$ implicitly places constraints on $\Delta G(j\omega)$ that must be adhered to in order to not violate (14). An extreme example would be that if $\Delta \beta(\omega) = 0$, then strictly speaking, $\Delta G(j\omega)$ would have to be selected such that $|\Delta E^i(\omega)| = 0$, $\forall i$, implying that there may be no design flexibility available.

To gain a handle on the incremental feedback controller change allowed, first-order Taylor series expansion is used to approximate the incremental error constraint as

$$\left| \Delta E^i \right| \approx \left| \frac{\partial E^i}{\partial g_a} \right|_{G_o, X_o} (g_a - g_{a0}) \Big|_{\omega} \leq \Delta \beta(\omega), \quad \forall a \in [1, m], \quad (23)$$

where $g_{a0}(j\omega)$ is the preliminary, known feedback controller design for row a , and $g_a(j\omega)$ is the corresponding, yet to be designed, updated feedback controller element. The structure in (23) allows for element-wise division by $\frac{\partial E^i}{\partial g_a} \Big|_{G_o, X_o, \omega}$.

Denoting $K_a^i(\omega) = \Delta \beta(\omega) \oslash \left| \frac{\partial E^i}{\partial g_a} \right|_{G_o, X_o, \omega}$, the constraint set on $g_a(j\omega)$ for plant instance i can be reposed as

$$\left| g_a - g_{a0} \right|_{\omega} \leq \min_{r, c \in [1, m]} k_{a, c}^i(\omega), \quad (24)$$

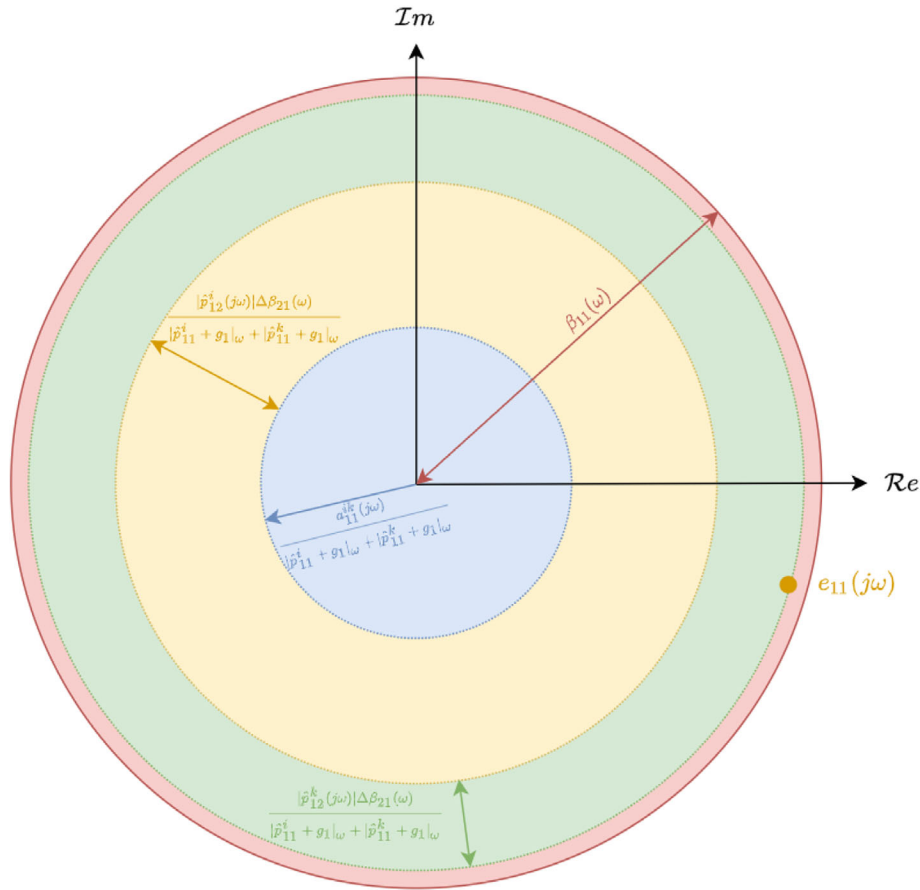


FIGURE 3 Arithmetic-complex plane showing geometric representation of the overbounded tracking error constraint from (20) for $\{r, c\} = \{1, 1\}$ of a 2×2 system. The sum of the terms on the left-hand side of (20) form a disc (green) that is required to lie within the tracking tolerance (red disc).

where \oslash is the Hadamard division operator. With reference to Figure 5, (24) describes a *stay-in* disc for $g_a(j\omega)$, with a center at $g_{a0}(j\omega)$ and a radius equal to the smallest element in $m \times m$ matrix $K_a^i(\omega)$ (as the intersection of the concentric *stay-in* discs will be equivalent to the disc with the smallest radius). In this way, the divergence of $g_a(j\omega)$ from the preliminary $g_{a0}(j\omega)$ is dictated by $\Delta\beta(\omega)$ (the incremental error magnitude allowed) and the element-wise reciprocal of $\left| \frac{\partial E^i}{\partial g_a} \right|_{G_0, X_0, \omega}$ (the sensitivity of the model tracking error with respect to the feedback controller element). Highly sensitive model tracking errors will then only allow small feedback controller adjustments and insensitive model tracking behavior will allow for larger controller gain/phase adjustments. $\Delta\beta(\omega)$ terms also appears on the left-hand side of (21), thereby enforcing an inherent trade-off between increasing the discoidal *stay-in* design regions of $g_a(j\omega)$ in (24) (by increasing $\Delta\beta(\omega)$), and decreasing the elliptical *stay-out* design regions from (21) (by decreasing $\Delta\beta(\omega)$). As evidenced in (21), the structure of hollow matrix $\left| \hat{P}_n^i \right|$ in (17) prevents row a elements of $\Delta\beta(\omega)$ from transitioning into row a of (17). This suggests that the designer can adjust specific elements of $\Delta\beta(\omega)$ to trade off design freedom between the different channels. This highlights an appealing aspect of this design approach—while the bound generation method is technically nonsequential, adjusting $\Delta\beta(\omega)$ enables prioritization of one loop over others on a perfrequency basis, which is made transparent by visualizing the feedback controller design regions in the log-polar plane. An example of the design region trade-off for a 2×2 system is shown in Figure 6. This method is conceptually similar to that of Reference 4, albeit framed in a model-error tracking context, with *a priori* gain-phase information also included in the updated design equations. Nominal selection of $\Delta\beta(\omega)$ is assisted by the tracking tolerance, $\beta(\omega)$, namely

$$\Delta\beta(\omega) = \lambda(\omega) \oslash \beta(\omega), \quad (25)$$

where $\lambda(\omega) \leq 1$ is a nonnegative matrix that is used to adjust element-wise values of $\Delta\beta(\omega)$, and \oslash is the Hadamard product operator. Note that $\beta(\omega)$ is used in the above formulation to provide appropriate weighting in terms of the original tracking specifications. $\lambda(\omega)$ is used to refine and trade the design regions across the various control loops. As an example,

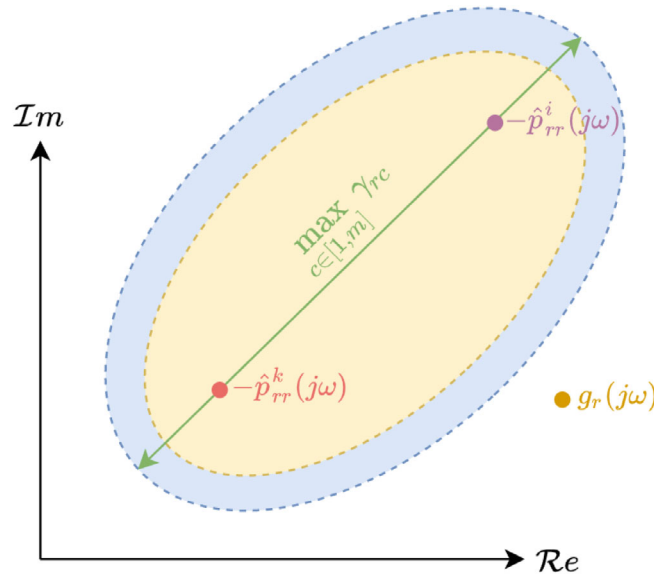


FIGURE 4 Arithmetic-complex plane showing elliptical *stay-out* design regions of $g_r(j\omega)$ for plant-pair $\{ik\}$, derived from (21), for a 2×2 plant. A valid $g_r(j\omega)$ is required to lie outside the union of the two ellipses with coincident foci, one resulting from each column in (17), which is equivalent to lying outside the larger blue ellipse. The blue ellipse is obtained directly from (22).

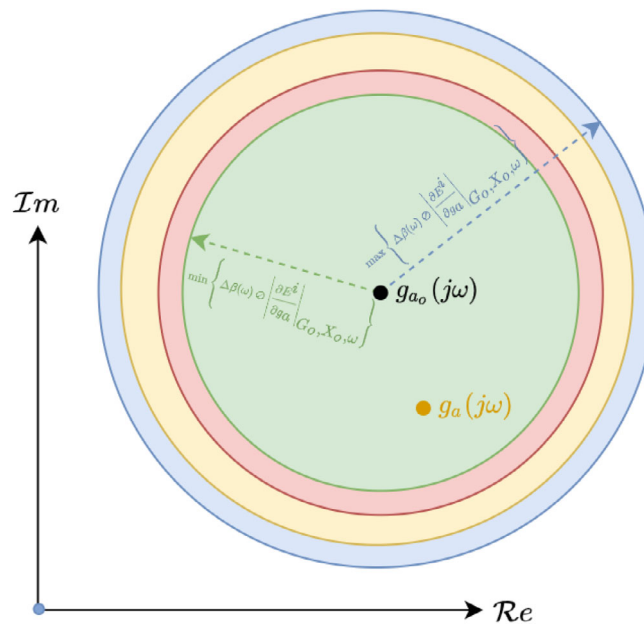


FIGURE 5 Geometric representation of (24) in the arithmetic-complex plane for an arbitrary 2×2 plant. The local solution space of $g_a(j\omega)$ for plant instance i is a *stay-in* disc that is dictated by the smallest (green) of the concentric discs centered at $g_{a_o}(j\omega)$. An $m \times m$ plant will result in m^2 concentric discs.

when designing $g_1(j\omega)$, one can shrink the *stay-out* ellipses from (21) by reducing $\lambda_{ab}(\omega)$, $a \neq 1$. However, the inherent reduction of $\Delta \beta_{ab}(\omega)$ means that the *stay-in* design region from (24) is likely to also shrink, thereby limiting the incremental design space of $g_2(j\omega)$. The designer is then tasked with finding a balance between the *stay-in* and *stay-out* design regions, which is facilitated by adjusting $\lambda(\omega)$ and then visualizing the resulting design region in the log-polar plane.

3.2.2 | Synthesizing $X_o(j\omega)$

Given that the magnitude of $|a_{rc}^{ik}(j\omega)|$ in (21) contributes to the size of the *stay-out* design regions, it is appealing and conceivable to minimize the worst-case magnitude of $|a_{rc}^{ik}(j\omega)|$ over all plant cases, which is equivalent to minimizing the

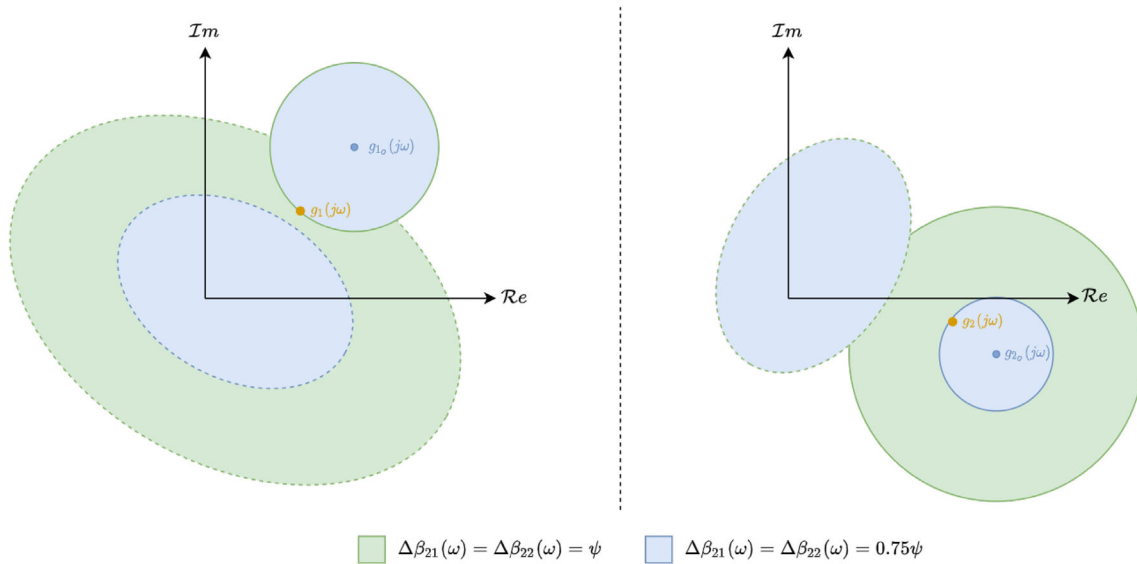


FIGURE 6 An example of the feedback controller design trade-off between $g_1(j\omega)$ (left) and $g_2(j\omega)$ (right), for a 2×2 plant, as a result of altering elements in the second row of $\Delta\beta(\omega)$. A valid feedback controller solution is required to lie outside of the ellipses from (21) (dashed lines) and within the discs from (24) (solid lines). Reducing $\Delta\beta_{21}(\omega)$ or $\Delta\beta_{22}(\omega)$ will reduce the size of the *stay-out* ellipses for $g_1(j\omega)$ based on (21) and Figure 4, but this may have the effect of reducing the discoidal *stay-in* design region of $g_2(j\omega)$ based on (24). Note that the *stay-in* discs of $g_1(j\omega)$ and *stay-out* ellipses of $g_2(j\omega)$ do not change as $\Delta\beta_{2k}(\omega)$ is reduced (the respective design regions are coincident).

first term in (17), $\left| \left(\hat{P}^i - \hat{P}^k \right) M + \hat{P}_n^k E_o^k - \hat{P}_n^i E_o^i \right|_\omega$, by adjusting $E_o(j\omega)$ using $X_o(j\omega)$ from (13). This would have the effect of increasing the admissible design region of $G(j\omega)$ constrained by (17), by reducing the major axes of the *stay-out* ellipses in (21). Setting $E_o^i(j\omega) = V_o^i(j\omega) - Z_o^i(j\omega)X_o(j\omega)$, (13) can be used to rewrite the first term of (17) as

$$\left| \left(\hat{P}^i - \hat{P}^k \right) M + \hat{P}_n^k E_o^k - \hat{P}_n^i E_o^i \right|_\omega = \left| \left(\hat{P}^i - \hat{P}^k \right) M + \hat{P}_n^k (V_o^k - Z_o^k X_o) - \hat{P}_n^i (V_o^i - Z_o^i X_o) \right|_\omega, \quad (26)$$

where $V_o^i(j\omega) = [I + P^i(j\omega)G_o(j\omega)]^{-1}M(j\omega)$, and $Z_o^i(j\omega) = [I + P^i(j\omega)G_o(j\omega)]^{-1}P^i(j\omega)$. The overarching minimax problem is to find a prototype $X_o(j\omega)$ such that (26) is element-wise minimized (in some sense), subject to the tracking error constraint in (3). One could also include the diagonal elements of $G_o(j\omega)$ as part of this free parameter set, but this has the risk of yielding a poorly-posed cost function. Denoting $Q_o^{ik}(j\omega) = \left(\hat{P}^i - \hat{P}^k \right) M + \hat{P}_n^k V_o^k - \hat{P}_n^i V_o^i$, and $R_o^{ik} = \hat{P}_n^k Z_o^k - \hat{P}_n^i Z_o^i$, the modulus of the (a, b) element in (26) is $\left| q_{ab}^i - \sum_{d=1}^m r_{ad}^i x_{db} \right|_\omega$. It follows that all the elements in column b of $X_o(j\omega)$ will appear in each element of column b of the set of resulting constraints (we cannot optimize for each element of $X_o(j\omega)$ individually). The adjusted minimax problem that finds all elements of $X_o(j\omega)$ in column b is

$$\{x_{1b}(j\omega), x_{2b}(j\omega), \dots, x_{mb}(j\omega)\} = \min \left\{ \max_{i \in [1, n]} \left\{ \sum_{a=1}^m \frac{|q_{ab}^i - \sum_{j=1}^m r_{aj}^i x_{jb}|_\omega}{\beta_{ab}(\omega)} \right\} \right\}, \quad (27)$$

where $\beta_{ab}(\omega)$ is used to weight the elements of column b based on the multivariable tracking priority. This is one approach to weighting the cost function in (27). Note that the structure in (27) is equivalent to

$$\{x_{1b}(j\omega), x_{2b}(j\omega), \dots, x_{mb}(j\omega)\} = \min \left\{ \max_{i \in [1, n]} \left\{ \sum_{a=1}^m \frac{|a_{ab}^{ik}|_\omega}{\beta_{ab}(\omega)} \right\} \right\}, \quad (28)$$

where $\frac{|a_{ab}^{ik}|_\omega}{\beta_{ab}(\omega)}$ is the first term in (21). In order to convert (27) into a form that can be interpreted by a constrained optimization routine, an additional free parameter, $\kappa_b(\omega) > 0$, is introduced, which replaces the objective function,

$$\{x_{1b}(j\omega), x_{2b}(j\omega), \dots, x_{mb}(j\omega)\} = \min \{\kappa_b(\omega)\}. \quad (29)$$

The required constraint that relates (29) to (27) is

$$\sum_{a=1}^m \frac{|q_{ab}^i - \sum_{k=1}^m r_{ak}^i x_{kb}|_{\omega}}{\beta_{ab}(\omega)} \leq \kappa_b(\omega), \quad \forall i \in [1, n]. \quad (30)$$

The objective is to minimize $\kappa_b(\omega)$, which in turn represents the maximum, or worst-case occurrence (it overbounds the plant-indexed set in question). In practice, each column element of $X_o(j\omega)$ is separated into the real-valued magnitude and phase components, $x_{ab}(j\omega) = R_{ab}(\omega)e^{j\theta_{ab}(\omega)}$, which necessitates the constraints, $R_{ab}(\omega) \geq 0$, $\theta_{ab}(\omega) \in [-\pi, \pi]$. Following this formulation, an $m \times m$ feedforward filter results in m optimization problems per frequency design point (one for each column), each with $2m + 1$ free parameters (two parameters for each element in a specific column of $X_o(j\omega)$ and one parameter for $\kappa_b(\omega)$ as detailed in (30)). The search space therefore increases linearly with m and does not suffer from higher-order scalability issues when handling plants with large dimensions.

3.2.3 | Generating the tracking design constraint set

Once $X_o(j\omega)$ has been synthesized, the resulting tracking error can be calculated using (13). Using knowledge of this prototype $E_o(j\omega)$ set, as well as defining the incremental error bounds from (24), the left-hand side of (21) is populated. Equation (21) and (24) are then used to generate the decoupled tracking design regions of the diagonal elements of $G(s)$. Note that when $|E_o^i(j\omega)| = 0$, $\forall i \in [1, n]$ (implying $\Delta\beta^i(\omega) = \beta^i(\omega)$), (12) and (17) become equivalent. This corresponds to the infinite feedback controller gain solution, which is analogous to having no a priori design information/insight.

The resulting plant-paired elliptical *stay-out* design regions from (21) are combined with the discoidal *stay-in* design regions from (24), which collectively determine the globally admissible solution space of $G(j\omega)$. As shown in Figure 7, the closed-form geometric structure of the individual design regions can be approximated by a polygon with sufficient boundary points. The intersection of all *stay-in* polygons will then define the resulting frequency-dependent design regions that can be visualized in the arithmetic-complex plane, or mapped to the log-polar plane. This is different to the traditional QFT approach of iteratively fixing the controller phase angle and then finding the roots of the polynomial that describes the underlying constraint at equality on the controller gain. The primary appeal in using polygonal approximations is in the way that the phase gridding is performed. With reference to Figure 7, the traditional approach approximates design regions by discretizing the continuous range of controller phase angles that span $[-\pi, \pi]$, and this has the potential to result in poorly approximated design regions, depending on the relative size and location of the design region. By stark contrast, discretization using triangular segments with a common point at the polygon center is less susceptible to underapproximation and requires less phase partitions to sufficiently capture an individual design region. This has the benefit of being computationally efficient, relative to traditional methods, and is more consistent in terms of the amount of conservatism present when approximating the design regions.

3.2.4 | Feedback control refinement via iteration

The procedure detailed from Section 3.2 to 3.2.3 may be iterated to try to improve on the feedback control design. A high-level summary of the algorithm is illustrated in Table 1. As indicated in Section 3.2.1, the model-error tracking sensitivity with respect to the controller elements will predominantly affect the number of iterations required when refining the feedback controller elements. That is, large incremental steps in the feedback controller are allowed when the sensitivity is low, but small increments are required when the sensitivity is relatively high. One approach is to set the elements in $\lambda(\omega)$ to be very small ($\lambda_{ab}(\omega) \ll 1$, $\forall \{a, b\} \in [1, m]$), which would allow small differential changes in $g_a(j\omega)$, based on (24), whilst simultaneously having reduced bound dominance from the elliptical *stay-out* tracking specification (the left-hand side of (17) would approach the nonconservative form). The obvious downside is that the increased number of design iterations would require longer time investment from the designer (as the bound generation routine would need to be executed repeatedly). It may be possible to automate the incremental controller refinements, but this is not investigated in this article.

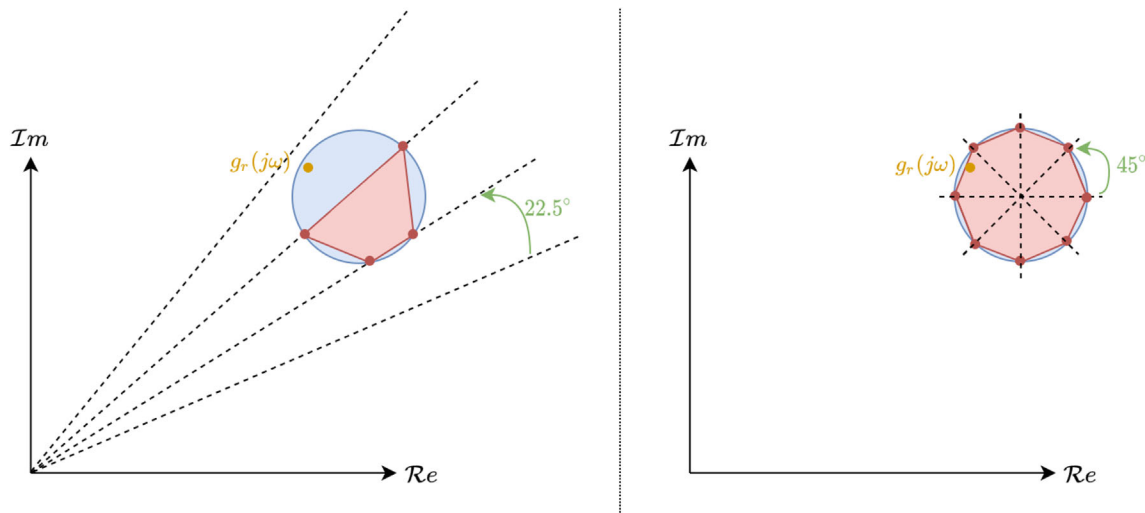


FIGURE 7 A graphical example of the mathematically derived (blue) and approximated (red) *stay-in* design regions, represented in the arithmetic-complex plane. The traditional QFT approach (left) grids the arithmetic-complex plane based on the phase angle of $g_r(j\omega)$. The mathematically derived design region (blue disc) is approximated by the quadrilateral polygon, which can exhibit large underapproximation. The proposed approach (right) grids the same design region using triangular segments that originate from the design region center. A valid $g_r(j\omega)$ is shown to lie in the blue disc, but it would be perceived as invalid when using traditional phase gridding with a 22.5° phase angle step.

TABLE 1 Iterative feedback control refinement algorithm

Step	Operation
1	Set current feedback controller iteration equal to valid <i>a priori</i> , design, e.g. based on Section 3.1: $G_o(s) \leftarrow G(s)$
2	Synthesize prototype $X_o(j\omega)$ using current $G_o(s)$, based on (29): $\{x_{1b}(j\omega), x_{2b}(j\omega), \dots, x_{mb}(j\omega)\} = \min \{\kappa_b(\omega)\}$
3	Select/adjust $\lambda(\omega)$ and update incremental tracking tolerance, as detailed in Section 3.2.1: $\Delta\beta(\omega) = \lambda(\omega) \odot \beta(\omega)$
4	Generate design regions for $G(j\omega)$ based on (21) and (24)
5	Return to Step 3 and refine $\lambda(\omega)$ if required, based on observation of design regions for $G(j\omega)$ in Step 4
6	Design $G(s)$ using design regions from Step 4
7	Update feedback controller prototype: $G_o(s) \leftarrow G(s)$
8	Return to Step 2 if further feedback controller shaping is required. Otherwise, end refinement process

Incremental refinement of the feedback controllers requires that the updated design constraints from (21) yield design regions that allow lower gain and more phase flexibility. Geometrically, this requires the elliptical stay-out regions from (21) to shrink in size (or at least the plant-pair-indexed ellipses that define the boundary conditions of the global *stay-out* design regions). As previously mentioned, setting $\Delta\beta(\omega) \rightarrow 0$ implies that the constraint set of (17) is nonconservative (as there is no gain and phase overbounding present in the constraint). Under these conditions, the feedforward filter synthesis step, from Section 3.2.2, will find a prototype $X_o(j\omega)$ that is not biased by conservatism from the triangle inequality, and will free up design space for the feedback controller elements, if it exists. Specifically, the left-hand side of (17) will continue to become smaller with each design iteration, allowing for iterative adjustment of $G(j\omega)$ on the corresponding right-hand side terms, until such time that application of (30) no longer shrinks the elliptical stay-out regions from (21).

3.3 | Feedforward filter design

Assuming a $G(s)$ can be designed that conforms to the aforementioned constraints in terms of the Bode gain-phase relationship, the final step is to design continuous $X(s)$. The proposed approach is to exploit the linear structure of the model tracking error constraint to define separate existence conditions on each column of $X(s)$. Defining (now known)

$V^i(j\omega) = [I + P^i(j\omega)G(j\omega)]^{-1}M(j\omega)$, and $Z^i(j\omega) = [I + P^i(j\omega)G(j\omega)]^{-1}P^i(j\omega)$, the model tracking error for plant i can be written as

$$E^i(j\omega) = V^i(j\omega) - Z^i(j\omega)X^i(j\omega). \quad (31)$$

Column c of $E^i(j\omega)$ can be written in expanded form as

$$E_{\{c\}}^i(j\omega) = V_{\{c\}}^i(j\omega) - Z^i(j\omega)X_{\{c\}}(j\omega) = V_{\{c\}}^i(j\omega) - \sum_{k=1}^m Z_{\{k\}}^i(j\omega)x_{kc}(j\omega), \quad (32)$$

where subscript $\{c\}$ indicates column (vector) c of a particular matrix. The corresponding element-wise design constraint follows as

$$\left| V_{\{c\}}^i - \sum_{k=1}^m Z_{\{k\}}^i x_{kc} \right|_{\omega} \leq \beta_{\{c\}}(\omega), \quad \forall i \in [1, n], \quad (33)$$

where $V_{\{c\}}^i(j\omega), Z_{\{k\}}^i(j\omega) \in \mathbb{C}^{m \times 1}$. Given that (33) must be satisfied for all plant cases ($\forall i \in [1, n]$), the above requirement can be reposed as

$$\left| \tilde{V}_{\{c\}}^1 - \sum_{k=1}^m \tilde{Z}_{\{k\}}^1 x_{kc} \right|_{\omega} \leq \tilde{\beta}_{\{c\}}(\omega), \quad (34)$$

where

$$\tilde{V}_{\{c\}}^1(j\omega) = \begin{bmatrix} V_{\{c\}}^1(j\omega) \\ V_{\{c\}}^2(j\omega) \\ \vdots \\ V_{\{c\}}^n(j\omega) \end{bmatrix} \in \mathbb{C}^{nm \times 1} \quad (35)$$

and

$$\tilde{Z}_{\{k\}}^1(j\omega) = \begin{bmatrix} Z_{\{k\}}^1(j\omega) \\ Z_{\{k\}}^2(j\omega) \\ \vdots \\ Z_{\{k\}}^n(j\omega) \end{bmatrix} \in \mathbb{C}^{nm \times 1} \quad (36)$$

are stacked vectors that comprise every plant-dependent instance for column c and k , respectively. Similarly, $\tilde{\beta}(j\omega) = \mathbf{I}_{(nm \times m)}\beta(j\omega)$, where $\mathbf{I}_{(nm \times m)}$ is an $nm \times m$ matrix that contains n vertically stacked $m \times m$ identity matrices. Equation (34) can be rewritten as

$$\left| \tilde{V}_{\{c\}}^1 - \sum_{k=1}^{m-1} \tilde{Z}_{\{k\}}^1 x_{kc} - \tilde{Z}_{\{m\}}^1 x_{mc} \right|_{\omega} \leq \tilde{\beta}_{\{c\}}^1(\omega) \quad (37)$$

without loss of generality. Following this, element-wise division on both sides of (37) by $\tilde{Z}_{\{m\}}^1(j\omega)$ exposes the design regions of $x_{mc}(j\omega)$, namely

$$\left| \tilde{V}_{\{c\}}^1 \oslash \tilde{Z}_{\{m\}}^1 - \sum_{k=1}^{m-1} \left[\tilde{Z}_{\{k\}}^1 \oslash \tilde{Z}_{\{m\}}^1 \right] x_{kc} - x_{mc} \mathbf{1}_{(nm \times 1)} \right|_{\omega} \leq \tilde{\beta}_{\{c\}}^1(\omega) \oslash \left| \tilde{Z}_{\{m\}}^1(j\omega) \right|, \quad (38)$$

where $\mathbf{1}_{(nm \times 1)}$ is an $nm \times 1$ column vector of ones. Each row of (38) describes an independent constraint on $x_{mc}(j\omega)$, which takes the geometric form of a discoidal *stay-in* design region in the arithmetic-complex plane. Specifically, the design region resulting from row a of (38) will have a center located at $\frac{\tilde{V}_{ac}^1 - \sum_{k=1}^{m-1} \tilde{Z}_{ak}^1 x_{kc}}{\tilde{Z}_{am}^1} \Big|_{\omega}$, with a corresponding radius equal to

$\frac{\tilde{\beta}_{ac}^1(\omega)}{|\tilde{Z}_{am}^1(j\omega)|}$. Ensuring a common intersection between any two *stay-in* discs, based on Figure 2, defines the necessary condition for the existence of a globally (across the entire plant set) feasible $x_{mc}(j\omega)$, which follows as

$$\left| \tilde{V}_{ac}^1 \oslash \tilde{Z}_{am}^1 - \tilde{V}_{bc}^1 \oslash \tilde{Z}_{bm}^1 - \sum_{k=1}^{m-1} \left(\left[\tilde{Z}_{ak}^1 \oslash \tilde{Z}_{am}^1 \right] - \left[\tilde{Z}_{bk}^1 \oslash \tilde{Z}_{bm}^1 \right] \right) x_{kc} \right|_{\omega} \leq \tilde{\beta}_{ac}^1(\omega) \oslash \left| \tilde{Z}_{am}^1 \right|_{\omega} + \tilde{\beta}_{bc}^1(\omega) \oslash \left| \tilde{Z}_{bm}^1 \right|_{\omega}, \quad (39)$$

where $\forall \{a, b\} \in [1, nm]$. Noting the structural similarities with (34), (39) can be written compactly as

$$\left| \tilde{V}_{\{c\}}^2 - \sum_{k=1}^{m-1} \tilde{Z}_{\{k\}}^2 x_{kc} \right|_{\omega} \leq \tilde{\beta}_{\{c\}}^2(\omega), \quad (40)$$

where row $r = 2(a - 1) + b$, column c of $\tilde{V}^2(j\omega)$, $\tilde{Z}^2(j\omega)$, and $\tilde{\beta}^2(\omega)$ are described respectively as

$$\tilde{V}_{rc}^2(j\omega) = \left[\tilde{V}_{ac}^1 \oslash \tilde{Z}_{am}^1 - \tilde{V}_{bc}^1 \oslash \tilde{Z}_{bm}^1 \right]_{\omega}, \quad (41)$$

$$\tilde{Z}_{rc}^2(j\omega) = \left[\tilde{Z}_{ac}^1 \oslash \tilde{Z}_{am}^1 \right]_{\omega} - \left[\tilde{Z}_{bc}^1 \oslash \tilde{Z}_{bm}^1 \right]_{\omega}, \quad (42)$$

and

$$\tilde{\beta}_{rc}^2(j\omega) = \tilde{\beta}_{ac}^1(\omega) \oslash \left| \tilde{Z}_{am}^1 \right|_{\omega} + \tilde{\beta}_{bc}^1(\omega) \oslash \left| \tilde{Z}_{bm}^1 \right|_{\omega}. \quad (43)$$

The number of combinations results in $\tilde{V}_{\{c\}}^2(j\omega)$, $\tilde{Z}_{\{c\}}^2(j\omega)$, $\tilde{\beta}_{\{c\}}^2(j\omega) \in \mathbb{C}^{n^2 m^2 \times 1}$, but after excluding redundant (repeated) combinations, there will actually be $nm(nm - 1)/2$ combinations. Referring to (40), one can then follow the same sequential procedure as in (37) and (38) to expose the design region of $x_{(m-1)c}(j\omega)$:

$$\left| \tilde{V}_{\{c\}}^2 \oslash \tilde{Z}_{\{m-1\}}^2 - \sum_{k=1}^{m-2} \left[\tilde{Z}_{\{k\}}^2 \oslash \tilde{Z}_{\{m-1\}}^2 \right] x_{kc} - x_{(m-1)c} \mathbf{1}_{(n^2 m^2 \times 1)} \right|_{\omega} \leq \tilde{\beta}_{\{c\}}^2(\omega) \oslash \left| \tilde{Z}_{\{m-1\}}^2(j\omega) \right|. \quad (44)$$

This method is applied $m - 1$ times in total to obtain the set of univariate design constraints on $x_{1c}(j\omega)$,

$$\left| \tilde{V}_{\{c\}}^m - x_{1c} \mathbf{1}_{(n^m m^m \times 1)} \right|_{\omega} \leq \tilde{\beta}_{\{c\}}^m(\omega). \quad (45)$$

All discoidal *stay-in* design regions of $x_{1c}(j\omega)$ in (45) must be satisfied simultaneously, which then gives rise to design regions of $x_{2c}(j\omega)$. Selecting a valid $x_{2c}(j\omega)$ then defines a nonempty design region for $x_{3c}(j\omega)$, and so on, until $x_{mc}(j\omega)$ is eventually designed. This constitutes sequentially chaining together existence conditions that informs the design of $x_{(k+1)c}$ based on the successive design choices for rows 1 to k . Importantly, the columns of $X(j\omega)$ are designed independently as there is no interaction in terms of meeting the tracking specifications (as evidenced by (32)). This approach is therefore applicable to arbitrarily large multivariable tracking designs and is equivalent to the bound generation routine outlined in Reference 9 when $m = 2$. Note that this feedforward design process is independent of the feedback control design routine that is applied. In other words, it can be incorporated into any 2DOF control design scheme. The feedforward filter row design order of $\{1 \rightarrow 2 \rightarrow \dots \rightarrow m\}$ is used here for sake of clarity, but the designer can choose the order in which the feedforward elements are designed based on the order in which existence conditions are specified. Changing the design order may have benefit in completing the design, but this is not included in this article.

4 | WORKED EXAMPLES

This Section provides solutions to two different benchmark problems^{10,16} with varying complexity and design requirements: the first to illustrate the method on a simple problem with only gain uncertainty; and the second, the

ill-conditioned distillation column. The emphasis is placed on the bound generation and analysis, with the controller design only included to illustrate that a causal, pragmatic control solution exists.

4.1 | Example 1: Benchmark problem with pure gain uncertainty

In order to demonstrate the efficacy of the proposed method, the proposed design routine is first applied to a fully specified problem,¹⁶ with an existing solution.¹⁰ The uncertain plant under consideration is

$$\mathbf{P}(s) = \frac{1}{s} \begin{bmatrix} k_{11} & k_{12} \\ k_{21} & k_{22} \end{bmatrix}, \quad \{k_{11}, k_{22}\} \in [2, 6], \quad \{k_{12}, k_{21}\} \in [0.5, 1.5], \quad (46)$$

which exhibits approximately 10 dB of gain uncertainty on each plant element and has an open-loop interaction index of ≤ 0.75 .¹⁷ The corresponding reference model and tracking error bounds, in the frequency band of $\omega \leq 10$ rad/s, are given as

$$M(s) = \text{diag} \left\{ \frac{1}{s/3 + 1}, \frac{1}{s/3 + 1} \right\}, \quad \beta_{ab}(\omega) = 0.2\omega\sqrt{1 + \omega^2/9}, \quad \forall \{a, b\} \in [1, 2]. \quad (47)$$

Additionally, the high frequency ($\omega \geq 10$ rad/s) sensitivity constraint is

$$\frac{1}{|1 + g_a/\hat{p}_{aa}^i|_\omega} \leq 4.5 \text{ dB}, \quad \forall i = \{1, 2, \dots, n\}. \quad (48)$$

A preliminary $G_o(s)$ is designed using the constraint set in (12), whilst also incorporating the high-frequency sensitivity specification in (48). With reference to Section 3.2.3, 360 boundary points are used to approximate each plant- or plant-paired-indexed design region resulting from (21) and (24). Appropriate union and intersect operations are then applied to the *stay-out* and *stay-in* polygonal approximations, respectively, which collectively forms the design space of $g_r(j\omega)$ within the arithmetic-complex plane. The design regions of the nominal open-loop transfer function are shown in the log-polar plane in Figure 8A, with

$$g_{10}(s) = 3.43 \frac{\frac{s}{22} + 1}{\left(\frac{s}{8.5} + 1\right) \left(\left(\frac{s}{40}\right)^2 + \frac{0.8s}{40} + 1\right)}. \quad (49)$$

Importantly, the arbitrarily selected nominal plant in Figure 8 of $P^0(s) = \frac{1}{s} \begin{bmatrix} 2 & 0.5 \\ 0.5 & 2 \end{bmatrix}$ has no effect on the solution space of $g_{10}(s)$ and is only included to preserve the traditional open-loop logarithmic gain-phase locus behavior. Note that Figure 8A and (49) also represent a valid design of nonsequentially designed $g_{20}(s)$, as the plant and tracking specifications, in (46) and (47) respectively, are symmetric.

With prototype $G_o(s) = \text{diag}\{g_{10}(s), g_{20}(s)\}$ defined, the feedforward filter synthesis proceeds as detailed in Section 3.2.2. Each column of $X_o(j\omega)$ is optimally selected based on the objective of minimizing the maximum of the weighted sum of the particular column's elements in (27), and this results in two optimization problems (one per column), with five parameters per optimization problem. $G_o(j\omega)$ and optimally selected $X_o(j\omega)$ are used to calculate the set of $E_o(j\omega)$, with $\lambda(\omega)$ initially set to 0.5. Following this, the design constraints in (21) and (24) are populated and yield *stay-out* and *stay-in* design regions on $G(j\omega)$, respectively. Referring to Table 1, $\lambda(\omega)$ is then adjusted until a satisfactory balance between the per-frequency *stay-out* and *stay-in* design regions are found. A refinement is then made to $G_o(s)$, with the objective of reducing the gain and phase at all frequencies. The refined feedback controller is then used to synthesize an updated $X_o(j\omega)$, which in turn gives rise to updated design constraints for $G_o(j\omega)$. The design regions in Figure 8B are the result of two refinement iterations, with an improved feedback controller solution of

$$g_1(s) = g_2(s) = 2.2 \frac{\frac{s}{11.26} + 1}{\left(\frac{s}{2.173} + 1\right) \left(\left(\frac{s}{22}\right)^2 + \frac{0.64s}{22} + 1\right)}, \quad (50)$$

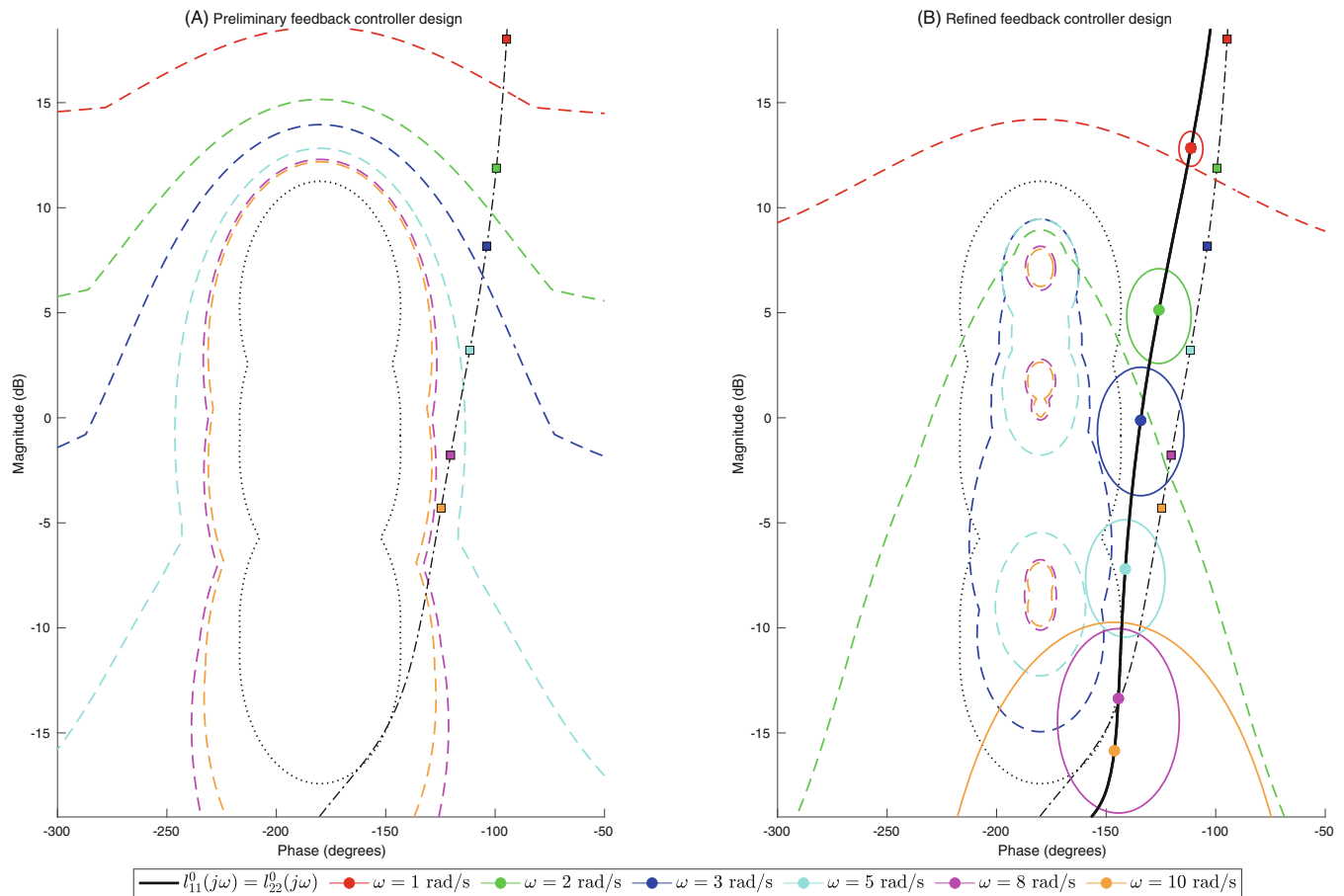


FIGURE 8 Universal *stay-out* sensitivity design regions (dotted line) and model-error tracking design regions on nominal loop transfer function, $l_{11}^0(j\omega) = \frac{2}{j\omega} g_1(j\omega)$ for (A) preliminary feedback controller design (dashed-dotted black line) using (12) and (B) refined feedback controller design (solid black line) using (21) and (24). The *stay-in* design regions from (24) are denoted with solid lines and the *stay-out* design regions from (12) and (21) are shown with dashed lines. The nominal open-loop loop transfer behavior from the preliminary design is also shown in (B) for sake of visual comparison.

TABLE 2 Frequency-dependent scaling parameters used when setting $\Delta\beta(\omega) = \lambda(\omega) \odot \beta(\omega)$ from (25)

ω (rad/s)	1	2	3	5	8	10
$\lambda_{ab}(\omega), \forall \{a, b\} \in [1, 2]$	0.1	0.3	0.4	0.4	0.16	0.135

Note: The symmetrical structure is a natural result of the symmetrical plant uncertainty and tracking specifications.

with the corresponding $\lambda(\omega)$ matrix and synthesized $X_o(j\omega)$ shown in Tables 2 and 3, respectively. The preliminary and adjusted feedback controller solutions are also shown in Figure 8B to illustrate the substantial relative gain/phase reduction after refining $G_o(s)$. The high-frequency sensitivity specifications from (48) are used as universal sensitivity constraints in the refined design (Figure 8B) to safeguard against undesirable sensitivity characteristics in the mid-frequency band ($\omega \in [2, 10]$). This was not required in the preliminary design as the tracking specifications from (12) dominated the gain-phase allowance (the sensitivity constraints were superseded by the mid- to high-frequency tracking constraints). This highlights the dramatic bound improvements from using *a priori* model-error tracking information. The relative gain and phase reductions in the refined feedback controller are significant, with frequency-dependent gain reductions in the feedback controllers of 4 to 10.3 dB, and phase reductions ranging from 16 to 29.4 degrees (for $\omega \in [1, 10]$).

Completing the 2DOF control scheme requires selecting a suitable $X(s)$ that adheres to the requirements in (3). This is facilitated using the procedure detailed in Section 3.3. Specifically, (45) is used directly to generate independent design regions for $x_{1c}(j\omega)$, $\forall c \in [1, 2]$, that must be satisfied simultaneously. Selection of a valid $x_{1c}(s)$ then engenders nonempty

TABLE 3 Synthesized $X_o(j\omega)$, after two iterations, using minimax procedure in Section 3.2.2

ω (rad/s)	1	2	3	5	8	10
$X_{11}(j\omega), X_{22}(j\omega)$	$0.0202 + 0.599j$	$-0.129 + 0.689j$	$0.128 + 0.115j$	$-0.305 + 0.072j$	-0.219	-0.314
$X_{12}(j\omega), X_{21}(j\omega)$	$0.073 - 0.455j$	$0.321 - 0.227j$	$0.439 + 0.355j$	$0.991 + 0.241j$	$1.168 + 0.358j$	$1.348 + 0.309j$

Note: The feedback controller from (50) is used to populate $V_o^i(j\omega)$ and $Z_o^i(j\omega)$ from (26).

design regions for the corresponding $x_{2c}(j\omega)$ element. Figure 9 shows the *stay-in* design regions of $X(s)$ in the log-polar plane of $\arg\{X(j\omega)\}$ versus $|X(j\omega)|_{\text{dB}}$. A viable, symmetrical, second-order solution of

$$X(s) = \begin{bmatrix} 0.66 \frac{s}{(s/2.5+1)(s/5+1)} & -0.46 \frac{s}{(s/3.4+1)(s/5.98+1)} \\ -0.46 \frac{s}{(s/3.4+1)(s/5.98+1)} & 0.66 \frac{s}{(s/2.5+1)(s/5+1)} \end{bmatrix} \quad (51)$$

is overlaid in Figure 9 and is shown to meet all frequency-dependent design regions. As highlighted in Reference 9, the feedforward structure in Figure 1 necessitates a feedforward filter with zero DC gain (i.e., derivative action), in order to achieve zero-error reference tracking at steady-state for *Type-0* feedback controllers, when considering step-like reference signals. The *stay-in* design regions in Figure 9 are smallest at the low frequencies (especially at $\omega = 1$ rad/s), which is related to how closely $G(j\omega)$ approached the frequency-dependent boundaries in Figure 8B. This is attributed to the fact that the design constraints on $g_a(j\omega)$ in (17) determine the existence of the corresponding $x_{ac}(j\omega)$ elements, and satisfying said constraint at equality for at least one plant instance causes the solution space of $x_{ac}(j\omega)$ to collapse to a point. By extension, setting $g_a(j\omega)$ such that the equality condition in (17) is approached will monotonically shrink the design region of $x_{ac}(j\omega)$. This, combined with the fact that design conservatism in (17) is most prevalent in the mid- to high-frequency band (as a result of the plant-inverting formulation) means that satisfying the low-frequency design frequency requirements for $X(j\omega)$ in Figure 9 are most challenging, but the high-frequency design becomes trivial. This illustrates the efficacy of the proposed feedforward design procedure in Section 3.3, as there is no reliance on conservative overbounding, such as the triangle inequality. Verification of meeting the tracking specifications in (3) is demonstrated by plotting the frequency response magnitude of the model-error tracking set against the tracking tolerance, as shown in Figure 10. The strict adherence to the model-error tracking tolerance in Figure 10 (within the low- to mid-frequency band where model tracking is prioritized) exemplifies the proposed method's ability to reduce design conservatism via iterative refinement and existential feedforward filter design.

4.2 | Example 2: Distillation column

The poorly conditioned distillation column problem¹⁸ is used as a final demonstration of the proposed method. The purpose is to focus less on the actual design and rather draw attention to the potential gain-phase saving, as well as the expanded solution spaces for both the feedback and feedforward control designs. The linearized plant is described by

$$P(s) = \frac{1}{1 + 75s} \begin{bmatrix} 0.878 & -0.864 \\ 1.082 & -1.096 \end{bmatrix} \begin{bmatrix} k_1 e^{-sT_1} & 0 \\ 0 & k_2 e^{-sT_2} \end{bmatrix}, \quad (52)$$

where $\{k_1, k_2\} \in [0.8, 1.2]$, and $\{T_1, T_2\} \in [0, 1]$ min, and has an open-loop interaction index of ≤ 0.985 .¹⁷ For sake of transparent bench-marking, the design specifications defined in Reference 10 are used in this worked example. The reference model specifications are

$$M(s) = \frac{1}{(\frac{s}{0.11})^2 + \frac{1.4s}{0.11} + 1} \begin{bmatrix} 1 & 0 \\ 0 & 1 \end{bmatrix}, \quad (53)$$

with the corresponding tracking tolerances detailed in Table 4. Note that for sake of clarity only a subset of the design frequency points in Table 4 were used. The robust stability specifications from Reference 10 follow as

$$\frac{1}{|1 + g_1/\hat{p}_{11}|_\omega} \leq 1.3 \text{ dB}, \quad \frac{1}{|1 + p_{11}g_1|_\omega} \leq 8 \text{ dB}, \quad (54)$$

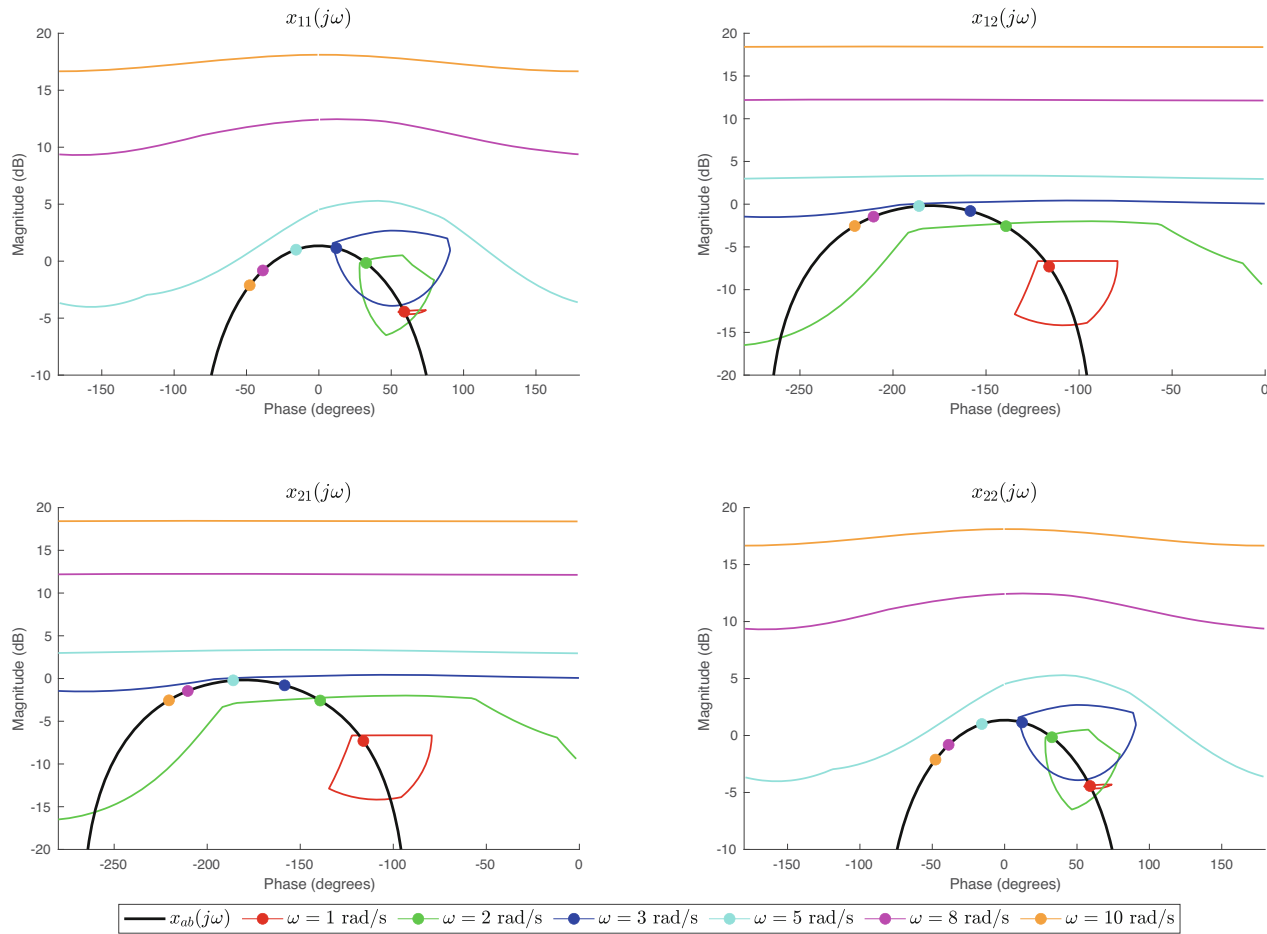


FIGURE 9 Stay-in design regions of $x_{ab}(j\omega)$ that arise from application of (45), described in the log-polar plane of $\arg\{x_{ab}(j\omega)\}$ versus $|x_{ab}(j\omega)|_{dB}$. $x_{12}(j\omega) = x_{21}(j\omega)$ is designed first, which dictates the corresponding solution space of $x_{11}(j\omega) = x_{22}(j\omega)$, based on satisfying the existence condition from (45).

and

$$\frac{1}{|1 + g_2/\hat{p}_{22}^*|_{\omega}} \leq 1.3 \text{ dB}, \quad (55)$$

where \hat{p}_{22}^* is detailed in Reference 10 as an equivalent plant that is used in the sequential design of $G(s)$ and includes information from $g_1(s)$. The solution from Reference 10, repeated in (56) below, is used as the preliminary design and represents an appropriate baseline to design from:

$$G_o(s) = \begin{bmatrix} \frac{2.2(0.008)(0.018)(0.45)(0.94,0.94)}{s(0.165)(0.25,0.64)(20,0.49)} & 0 \\ 0 & \frac{-3(0.02)(0.8)(3.2)(0.7,0.4)}{s(0.4)(10)(10)(0.24,0.65)} \end{bmatrix}, \quad (56)$$

where the short-hand notation of (a) and (b, c) corresponds to $(s/a + 1)$ and $(s^2/b^2 + 2cs/b + 1)$, respectively.

Using the preliminary feedback controller design in (56), and noting that the existence of a corresponding valid $X_o(s)$ is ratified based on the completed solution in Reference 10, a prototype $X_o(j\omega)$ is synthesized using (30). The procedure detailed in Table 1 is followed, whereby $G_o(s)$ and $X_o(j\omega)$ are iteratively designed and synthesized, respectively, with $\lambda(\omega)$ used to trade design strictures between the two control channels. This is especially invaluable in the distillation column problem, as the two channels have fundamentally different gain-phase requirements (which was not the case for the symmetrical benchmark example in Section 4.1). Equation (55) is a function of selected $g_1(j\omega)$ and is reevaluated after each iteration to update the stability requirements of $g_2(j\omega)$. As in Section 4.1, 360 boundary points are used when forming the

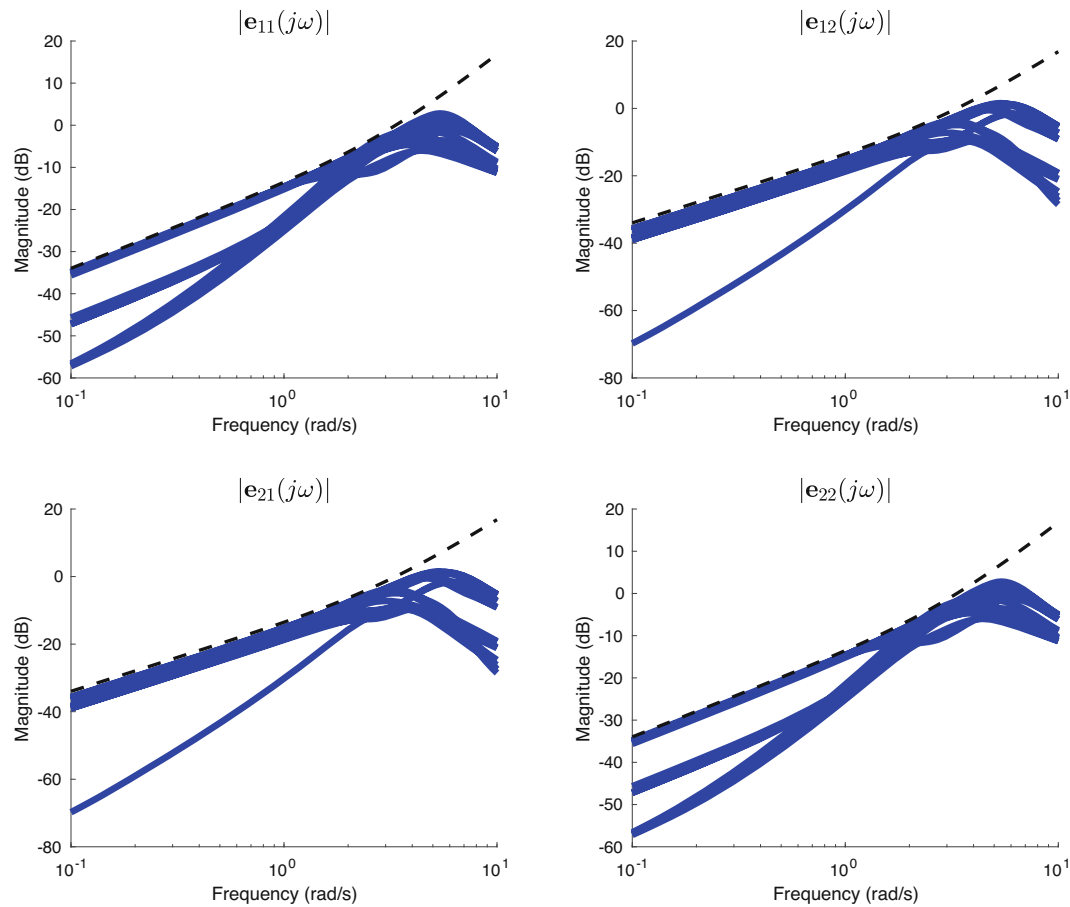


FIGURE 10 Bode magnitude plot showing 2×2 model-error tracking set (blue) from (4) and its adherence to the prescribed tracking tolerance (dashed black line) in (47).

TABLE 4 Discrete tracking tolerances at chosen design frequencies from Reference 10

ω	0.01	0.02	0.04	0.055	0.08	0.1	0.13	0.15	0.2	0.3	0.4	0.5	1	1.5
$\beta_{11}(\omega)$	0.12	0.2	0.33	0.48	0.6	0.6	0.6	0.6	0.6	0.6	0.5	0.65	0.58	0.5
$\beta_{12}(\omega)$	0.5	0.5	0.5	0.5	0.5	0.5	0.5	0.5	0.5	0.5	0.5	0.5	0.55	0.55
$\beta_{21}(\omega)$	0.5	0.5	0.5	0.5	0.5	0.5	0.5	0.5	0.4	0.4	0.45	0.6	0.7	0.6
$\beta_{22}(\omega)$	0.1	0.1	0.15	0.25	0.3	0.3	0.32	0.33	0.33	0.31	0.43	0.55	0.65	0.65

Note: The frequency is expressed in radians per minute. Boldface entries denote the design frequencies and corresponding tracking tolerances that are used in Figure 11.

polygonal approximations that define the individual design regions. The resulting nominal loop transfer design regions are shown in Figure 11 after two refinement iterations, with the corresponding feedback controller solution of

$$G(s) = 0.6G_o(s) = \begin{bmatrix} \frac{1.32(0.008)(0.018)(0.45)(0.94,0.94)}{s(0.165)(0.25,0.64)(20,0.49)} & 0 \\ 0 & \frac{-1.8(0.02)(0.8)(3.2)(0.7,0.4)}{s(0.4)(10)(10)(0.24,0.65)} \end{bmatrix}, \quad (57)$$

and corresponding prototype feedforward filter as shown in Table 5. Note that arbitrarily selected $P^0(s) = \frac{0.8}{1+75s} \begin{bmatrix} 0.878 & -0.864 \\ 1.082 & -1.096 \end{bmatrix}$ is used to display the nominal open-loop design regions in Figure 11. The corresponding $\lambda(\omega)$ values are shown in Table 6. Note that for sake of simplicity, only the gain of $G(s)$ was altered when performing the design refinements. Importantly, the reduced gain solution in (57) and Figure 11 (4.44 dB gain reduction) could have been

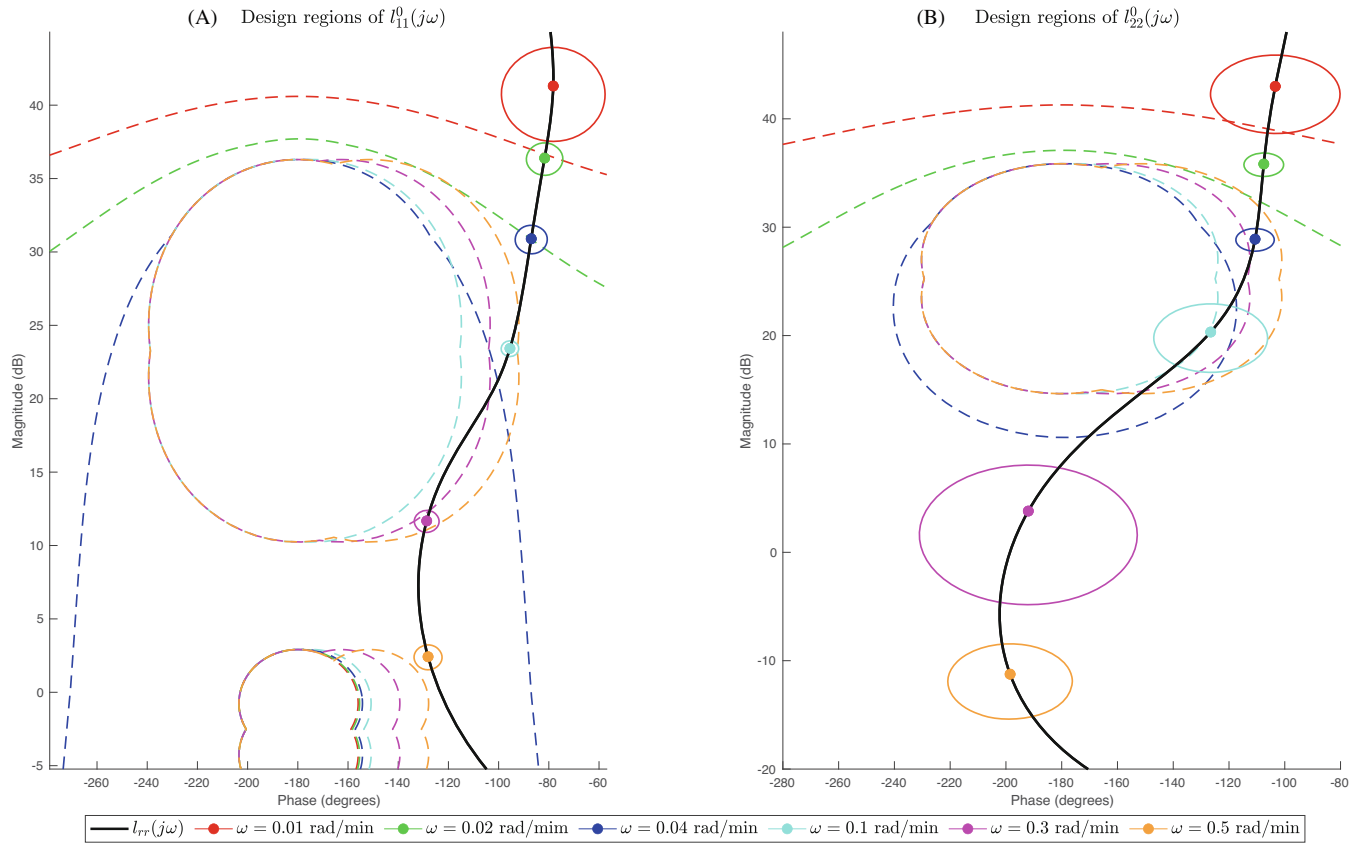


FIGURE 11 Log-polar plane showing the design regions, from (21), (54), and (55), on (a) nominal loop transfer function, $l_{11}^0(j\omega) = \frac{0.7024}{75\omega+1}g_1(j\omega)$ and (b) nominal loop transfer function, $l_{22}^0(j\omega) = -\frac{0.88}{75\omega+1}g_2(j\omega)$. Stay-out design regions (intersection of tracking and stability requirements) are depicted with dashed lines and stay-in design boundaries from (24) are shown with solid lines. For sake of clarity, a subset of the design frequencies from Table 4 are shown.

further refined, but the allocated headroom (meeting the requirements in (17) away from equality) allows for additional design freedom when shaping $X(s)$, based on the existential link between the feedback controller and feedforward filter.

Following the successful design of $G(s)$, the feedforward filter is designed as detailed in Section 3.3. The resulting design regions are shown in Figure 12, overlaid with a valid solution of

$$X(s) = \begin{bmatrix} \frac{37.57(0.036)}{(0.113, 0.41)} & \frac{86.14(0.055, 0.5)}{(0.02)(0.55, 0.31)(0.11, 0.3)} \\ \frac{2233s(0.13, 0.43)(0.63, 0.38)}{(0.69, 0.83)(0.13, 0.32)(0.08, 0.64)} & \frac{-12.13(0.011)(0.37, 0.19)}{(0.24)(0.14)(0.26, 0.90)(0.37, 0.50)} \end{bmatrix}. \quad (58)$$

As noted in References 9 and 10, the span of the frequency-dependent design regions in Figure 12 are directly dictated by emphasizing (or de-emphasizing) the disturbance rejection characteristics over the model-error tracking characteristics. In other words, overdesigning the feedback controllers in Figure 11 would lead to larger design regions on the feedforward filter, based on the existence conditions in (17), whereas minimum gain-phase design of the feedback controller results in heavily constrained prefilter shaping flexibility. The latter case can be seen in the second row of Figure 12, at the mid-frequencies. Given that the feedforward filter design procedure outlined in Section 3.3 is also facilitated by existence conditions, the selection of $x_{1b}(j\omega)$ in Figure 12 ultimately determines the corresponding $x_{2b}(j\omega)$ solution space based on how strictly the necessary condition in (45) is adhered to. The designer is therefore required to constantly allocate additional headroom to all interim controller designs, in order to prevent subsequent loop shaping issues as a result of the Bode gain-phase relationship. An appealing option could be to incorporate filter synthesis from Reference 19, which would theoretically allow for lower gain-phase feedback controller solutions, but this is not encapsulated in the scope of this article.

The frequency-based design routine is ratified in Figure 13 by comparing the modulus of the model-error tracking behavior with the tracking specifications in Table 4. The proposed nonconservative feedforward filter design methodology

TABLE 5 Synthesized $X_o(j\omega)$, after two iterations, using minimax procedure in Section 3.2.2

ω (rad/min)	0.01	0.02	0.04	0.1	0.3	0.5
$X_{11}(j\omega)$	14.315 − 36.413j	7.707 − 53.387j	2.827 − 75.054j	25.339 − 95.259j	16.153 + 3.004j	3.173 + 1.264j
$X_{12}(j\omega)$	54.902 + 88.736j	48.216 + 73.299j	31.342 + 81.438j	−16.403 + 79.710j	−10.767 − 0.924j	−1.117 × 10 ^{−6} − 1.857 × 10 ^{−8} j
$X_{21}(j\omega)$	−8.359 − 1.084j	−2.979 − 80.971j	12.242 − 77.853j	25.506 − 14.437j	1.113 × 10 ^{−6} + 8.128 × 10 ^{−7} j	7.682 × 10 ^{−7} − 4.351 × 10 ^{−7} j
$X_{22}(j\omega)$	−14.397 + 26.208j	−12.636 + 25.641j	−17.720 + 35.710j	−25.733 + 8.768j	−1.462 − 2.808j	0.021 − 0.567j

Note: The feedback controller from (50) is used to populate $V_o'(j\omega)$ and $Z_o'(j\omega)$ from (26).

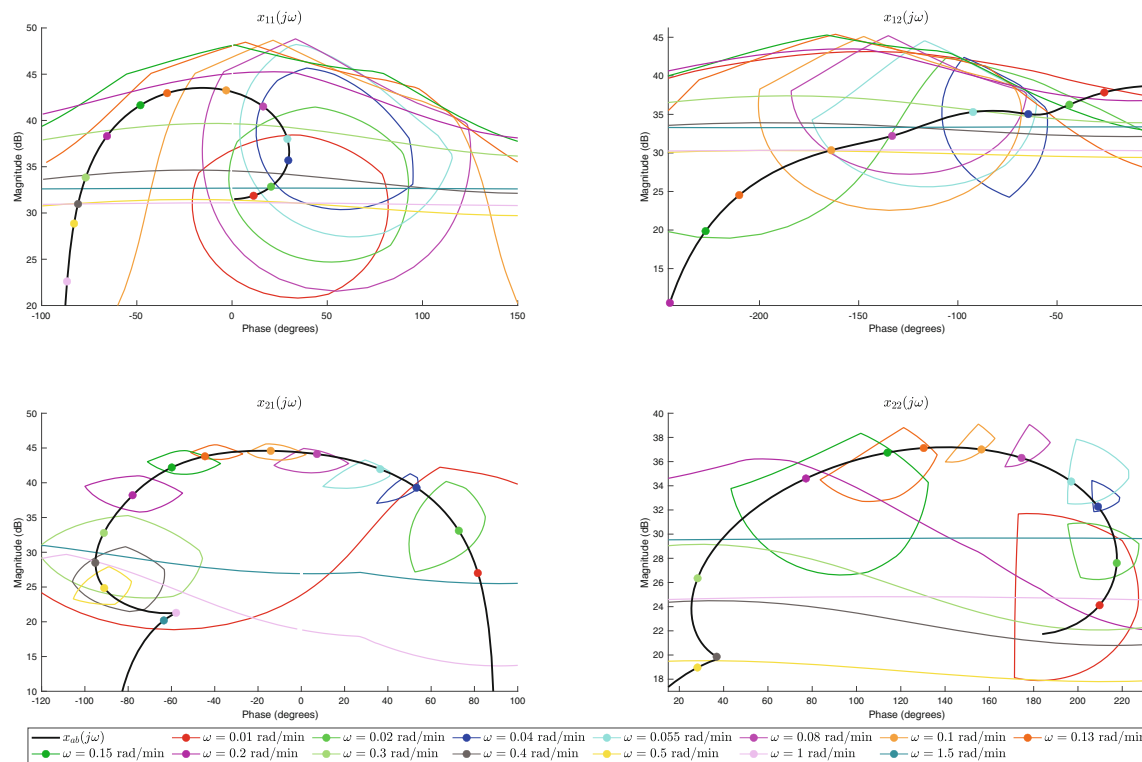


FIGURE 12 Stay-in design regions of $x_{ab}(j\omega)$, described in the log-polar plane of $\arg\{x_{ab}(j\omega)\}$ versus $|x_{ab}(j\omega)|_{\text{dB}}$. The $x_{1b}(j\omega)$ elements are designed first, which gives rise to valid solution spaces for the $x_{2b}(j\omega)$ elements, based on satisfying the existence condition from (45).

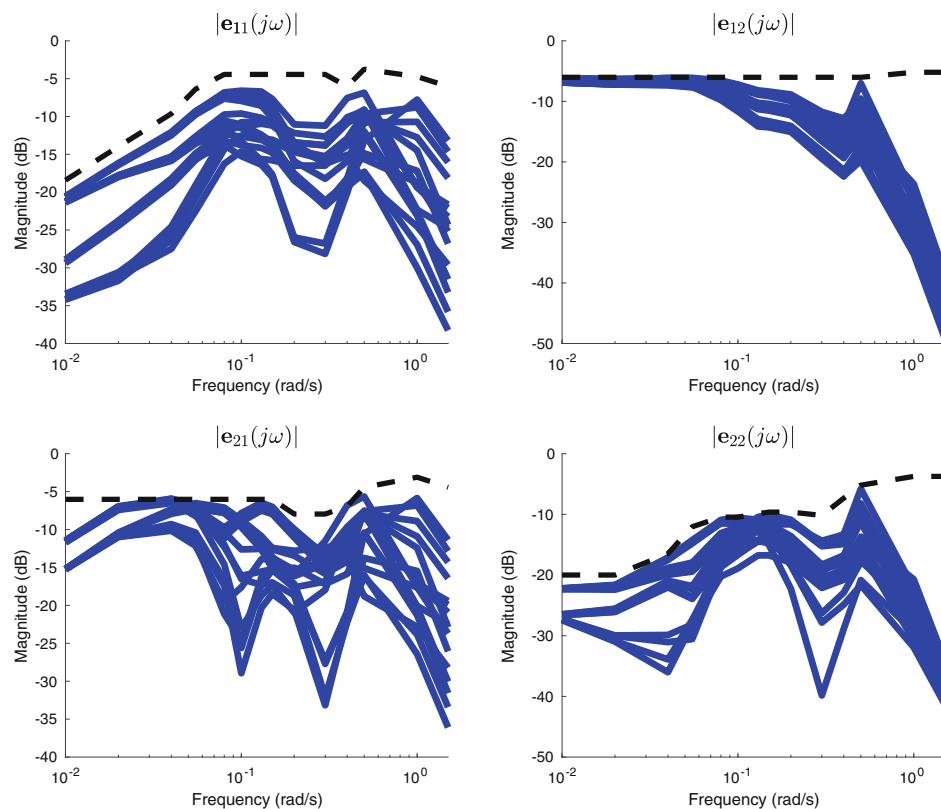
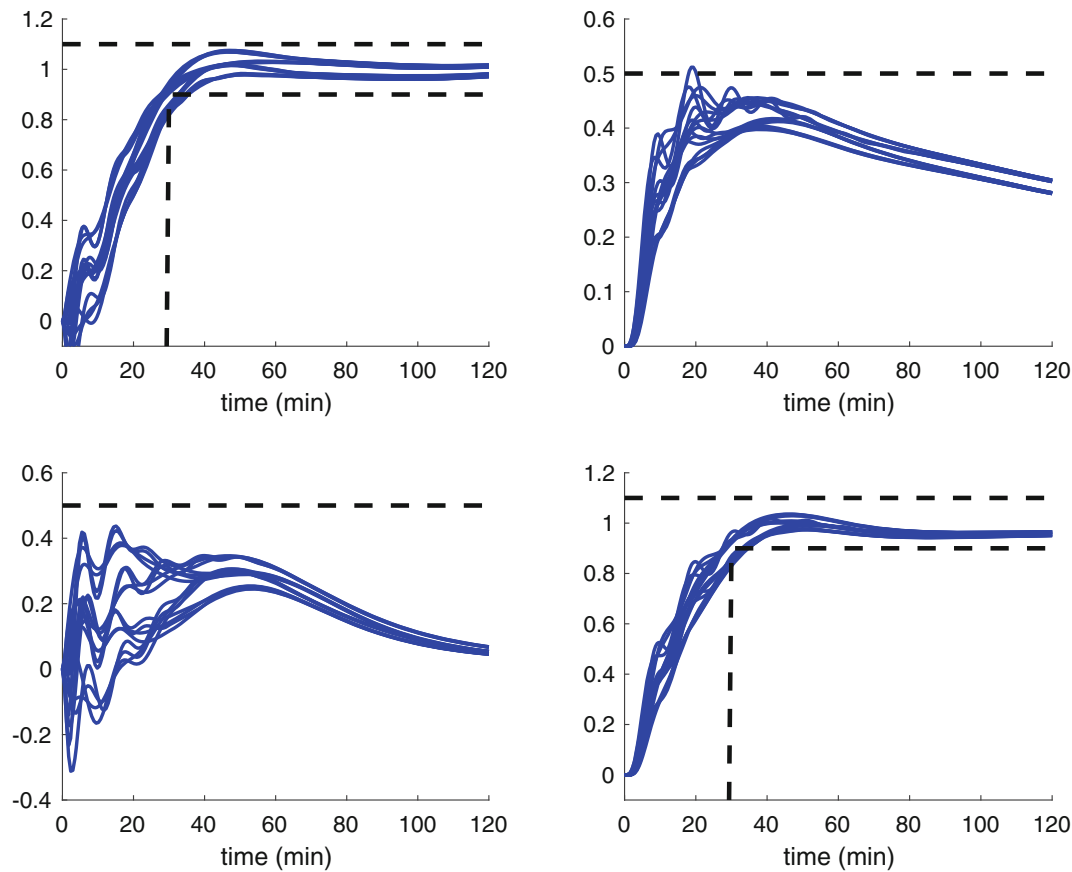


FIGURE 13 Bode magnitude plot showing 2×2 model-error tracking set (blue) from (4) and its adherence to the prescribed tracking tolerances (dashed black) in Table 4

TABLE 6 Frequency-dependent scaling parameters used when setting $\Delta\beta(\omega) = \lambda(\omega) \odot \beta(\omega)$ from (25)

ω (rad/min)	0.01	0.02	0.04	0.1	0.3	0.5
$\lambda_{11}(\omega), \lambda_{12}(\omega)$	0.35	0.1	0.075	0.3	0.15	0.1
$\lambda_{21}(\omega), \lambda_{22}(\omega)$	0.5	0.5	0.5	0.1	0.05	0.025

**FIGURE 14** Element-wise step responses of closed-loop plant set. The time-domain specifications from Reference 18 are also shown for sake of completeness. Minor violations of the time-domain requirements can be seen, which would ordinarily necessitate tightening of the tracking tolerances.

is exemplified by the fact that selection of an $x_{ab}(j\omega_d)$ lying on the edge of the *stay-in* design region at $\omega = \omega_d$ (in Figure 12) will result in $\beta_{cb}(j\omega_d) \in |\mathbf{e}_{cb}(j\omega_d)|$, where row c is dictated by the most stringent constraint in (33). An example of this is at $\omega = 0.1$ rad/min, whereby $x_{22}(j0.1)$ lies on the edge of the *stay-in* design region in Figure 12 and results in $\beta_{22}(j0.1) \in |\mathbf{e}_{22}(j0.1)|$, as shown in Figure 13. For sake of completeness, the time-domain unit step responses of the closed-loop plant set are shown in Figure 14. Note that the purpose of this paper is not to demonstrate strict adherence to the time-domain tracking specifications from Reference 18, but to rather show that the frequency-domain specifications from Reference 10 are enforced with reduced overdesign, as evidenced in 13.

5 | CONCLUSION

This article has presented a new, iterative feedback controller refinement approach to multivariable model-error tracking design problems. Additionally, a generalized feedforward filter design routine has been proposed that does not rely on the triangle inequality and assists in reducing the feedback controller gain-phase requirements. This combined method has been applied to two 2×2 benchmark problems of varying complexity and design requirements, and was shown to significantly reduce the gain and phase requirements of the feedback controller across all relevant design frequencies.

CONFLICT OF INTEREST


The authors declare no potential conflict of interest.

DATA AVAILABILITY STATEMENT

The functions and algorithms used during the current study are available from the corresponding author on reasonable request.

ORCID

Arnold Pretorius  <https://orcid.org/0000-0002-1940-588X>

Edward Boje  <https://orcid.org/0000-0003-2733-3537>

REFERENCES

- Horowitz IM. *Synthesis of Feedback Systems*. Elsevier; 2013.
- Horowitz I. Quantitative synthesis of uncertain multiple input-output feedback system. *Int J Control*. 1979;30(1):81-106.
- Boje E. Multivariable quantitative feedback design for tracking error specifications. *Automatica*. 2002;38(1):131-138.
- Rico J, Gil-Martinez M. Multivariable QFT robust control of a heat exchanger. Proceedings of the 2011 19th Mediterranean Conference on Control & Automation (MED); 2011:588-593.
- Garcia-Sanz M. *Robust Control Engineering: Practical QFT Solutions*. CRC Press; 2017.
- Bailey F, Hui CH. Cacs tools for loop gain-phase shaping design of SISO robust controllers. Proceedings of the IEEE Control Systems Society Workshop on Computer-Aided Control System Design; 1989:151-157; IEEE.
- Eitelberg E. Quantitative feedback design for tracking error tolerance. *Automatica*. 2000;36(2):319-326.
- Boje E. Pre-filter design for tracking error specifications in QFT. *Int J Robust Nonlinear Control IFAC-Affiliat J*. 2003;13(7):637-642.
- Pretorius A, Boje E. A complementary quantitative feedback theory solution to the 2x2 tracking error problem. *Int J Robust Nonlinear Control*. 2020;30(16):6569-6584.
- Elso J, Gil-Martinez M, Garcia-Sanz M. A quantitative feedback solution to the multivariable tracking error problem. *Int J Robust Nonlinear Control*. 2014;24(16):2331-2346.
- Elso J, Gil-Martinez M, Garcia-Sanz M. Quantitative feedback control for multivariable model matching and disturbance rejection. *Int J Robust Nonlinear Control*. 2017;27(1):121-134.
- Shaked U, Horowitz I, Golde S. Synthesis of multivariable, basically non-interacting systems with significant plant uncertainty. *Automatica*. 1976;12(1):61-71.
- Yaniv O. *Quantitative Feedback Design of Linear and Nonlinear Control Systems*. Vol 509. Springer Science & Business Media; 2013.
- Horowitz I. Survey of quantitative feedback theory (QFT). *Int J Robust Nonlinear Control IFAC-Affiliat J*. 2001;11(10):887-921.
- Elso J, Gil-Martinez M, Garcia-Sanz M. Quantitative feedback-Feedforward control for model matching and disturbance rejection. *IET Control Theory Appl*. 2013;7(6):894-900.
- Yaniv O, Chait Y. A simplified multi-input multi-output formulation for the quantitative feedback theory. Proceedings of the 1991 American Control Conference; 1991:1995-2000.
- Boje E. Non-diagonal controllers in MIMO quantitative feedback design. *Int J Robust Nonlinear Control IFAC-Affiliat J*. 2002;12(4):303-320.
- Limebeer D. The specification and purpose of a controller design case study. Proceedings of the 30th IEEE Conference on Decision and Control; 1991:1579-1580; IEEE.
- Elso J, Ostolaza JX. Automatic synthesis of feedforward elements in quantitative feedback theory. *Int J Robust Nonlinear Control*. 2021;31(12):5525-5540.

How to cite this article: Pretorius A, Boje E. A refinement approach to the multivariable tracking error problem. *Int J Robust Nonlinear Control*. 2022;32(12):7016-7038. doi: 10.1002/rnc.6183